PHYSICAL REVIEW C VOLUME 43, NUMBER 3 MARCH 1991

Radiative muon capture on carbon, oxygen, and calcium

D.S. Armstrong,[a] S. Ahmad,[b] R.A. Burnham,[c] T.P. Gorringe,[d] M.D. Hasinoff, A.J. Larabee,[e] and C.E. Waltham
University of British Columbia, Vancouver, British Columbia, Canada V6T 2A6

G. Azuelos,[f] J.A. Macdonald, T. Numao, and J-M. Poutissou
TRIUMF, Vancouver, British Columbia, Canada V6T 2A3

M. Blecher and D.H. Wright[g]
Virginia Polytechnic Institute and State University, Blacksburg, Virginia 24061

E.T.H. Clifford[h] and J. Summhammer[i]
TRIUMF and University of Victoria, Victoria, British Columbia, Canada V8W 2Y2

P. Depommier and R. Poutissou
Université de Montréal, Montréal, Québec, Canada H3C 3J7

H. Mes
National Research Council of Canada, Ottawa, Canada K1A OR6

B.C. Robertson
Queen's University, Kingston, Ontario, Canada K7L 3N6
(Received 9 May 1990)

The photon energy spectra from radiative muon capture on ^{12}C, ^{16}O, and ^{40}Ca have been measured using a time projection chamber as a pair spectrometer. The branching ratio for radiative muon capture is sensitive to g_p, the induced pseudoscalar coupling constant of the weak interaction. Expressed in terms of the axial-vector weak coupling constant g_a, values of $g_p/g_a = 5.7 \pm 0.8$ and $g_p/g_a = 7.3 \pm 0.9$ are obtained for ^{40}Ca and ^{16}O, respectively, from comparison with phenomenological calculations of the nuclear response. From comparison with microscopic calculations, values of $g_p/g_a = 4.6 \pm 1.8$, $13.6\ ^{+1.6}_{-1.9}$, and $16.2\ ^{+1.3}_{-0.7}$ for ^{40}Ca, ^{16}O, and ^{12}C, respectively, are obtained. The microscopic results are suggestive of a renormalization of the nucleonic form factors within the nucleus.

I. INTRODUCTION

In a general semileptonic weak process, the strong interaction induces additional couplings besides the standard vector and axial-vector terms. These couplings all appear in the effective Hamiltonian in terms proportional to the momentum transfer q. Muon capture ($\mu^- + p \rightarrow \nu_\mu + n$), with its characteristically large momentum transfer, has been the process of choice for investigating these induced couplings. The induced tensor coupling is expected to be zero due to G invariance, and likewise the induced scalar interaction is expected to vanish due both to the conserved vector current hypothesis (CVC) and G invariance. CVC also allows the induced magnetic form factor to be related to electromagnetic form factors, and in the limit of $q^2 \rightarrow 0$ it can be expressed in terms of the anomalous magnetic moments of the nucleons. The remaining term, the induced pseudoscalar coupling g_p, is not so well predicted theoretically. Through the use of the partially conserved axial-vector current hypothesis (PCAC), one obtains the estimate g_p/g_a=6.8 for the nucleon, at the momentum transfer corresponding to ordinary muon capture, where g_a is the axial-vector coupling constant. The world average of recent measurements of the rate of ordinary (nonradiative) muon capture (OMC) on hydrogen yields a value for g_p/g_a of 6.9 ± 1.5,[1] in good agreement with the PCAC prediction. However, the individual measurements which contribute to this average each have errors in excess of ±40%.

A small contribution ($\sim 10^{-4}$) to muon capture occurs via the process

$$\mu^- p \rightarrow n \nu_\mu \gamma \quad , \tag{1}$$

known as radiative muon capture (RMC). In this case, unlike OMC, the momentum transfer is not fixed, but varies between $q^2 = -0.9 m_\mu^2$ and $q^2 = +m_\mu^2$. Since the pseudoscalar contribution is dominated by the one-pion-exchange diagram, the effect of g_p is enhanced for momentum transfers near the pole in the pion propagator, i.e., near the high-energy end of the photon spectrum.

This increased sensitivity to g_p is the main reason that RMC has become the preferred method for measuring g_p. The low capture probability in hydrogen ($\sim 10^{-3}$) combined with the low expected radiative branching ratio ($\sim 10^{-5}$) has thus far precluded a measurement of the elementary radiative capture process [Eq. (1)].

RMC measurements are less difficult for heavier nuclei where the muon capture probability is greatly enhanced. Nuclear RMC may also reveal modifications of the elementary process by non-nucleonic degrees of freedom in the nucleus, which could manifest themselves as a renormalization of g_p. Exclusive nuclear RMC, i.e., to a specific final nuclear state, has not yet been attempted, and would pose formidable experimental challenges. All measurements of RMC to date have been inclusive ones, in which the final nuclear states were not experimentally resolved. These suffer the disadvantage that the nuclear response function must be correctly accounted for. Meaningful interpretation of such measurements is therefore restricted to well-understood nuclei such as ^{40}Ca. This sensitivity to nuclear structure can be reduced (but not eliminated) by considering the branching ratio RMC/OMC. If the experimental result is compared to the prediction of a calculation in which the RMC and OMC rates are estimated in a consistent way, some of the sensitivity to the nuclear matrix elements can be expected to cancel.

The first observation of RMC was by Conforto, Conversi, and di Lella in 1962[2] using an Fe target. Various early measurements of RMC using NaI detectors encountered difficulties due to neutron-induced backgrounds. This problem has recently been overcome through the use of photon converters, either along with a NaI detector[3–5] or a small solid-angle pair spectrometer.[6] Only for ^{40}Ca is there good agreement on the RMC/OMC branching ratio from different experiments,[3–6] the four recent measurements all yielding values consistent with an integrated yield of 2.1×10^{-5} for photons with energies greater than 57 MeV. For ^{16}O the situation is not as clear: Two existing measurements[4,7] provide branching ratios that differ from each other by more than 3σ. The branching ratio for ^{12}C has been measured,[4] however, with large (67%) errors, and the same group has measured RMC on ^{27}Al, ^{nat}Fe, ^{165}Ho, and ^{209}Bi. The latter results indicate an interesting systematic reduction in the RMC branching ratio with increasing atomic number.

The present paper reports a measurement of the rate of inclusive radiative muon capture on three nuclei: ^{40}Ca, ^{16}O, and ^{12}C. For the ^{40}Ca and ^{12}C targets data were taken in two different runs using photon converters of different thickness. The results for ^{16}O have been published previously[8] but are presented here in more detailed form. Preliminary results on all three nuclei have been presented elsewhere.[9,10]

II. THEORETICAL MODELS

The problem of calculating the various observables for RMC on complex nuclei can be divided into two stages. The first stage is the determination of the amplitude for the elementary process $\mu^- p \rightarrow n\nu_\mu\gamma$. Several different approaches[11–15] to the determination of this amplitude now appear to yield consistent results,[16–18] except for higher-order terms which typically affect the RMC rate at the level of a few percent.

The second, and more problematic stage, is that of "embedding" the elementary amplitude within the nucleus and accounting for the effects of nuclear structure. To date, the majority of the nuclear RMC calculations have adopted the impulse approximation, in which the amplitude for the elementary process is summed incoherently over all the nucleons in the nucleus. In this approximation, interactions involving more than one nucleon are neglected, i.e., meson-exchange currents are not included. Even within the impulse approximation, the calculation is non-trivial, since the RMC amplitudes must be summed over all possible final states. The earliest method adopted for this final-state summation was the closure approximation,[13,19,20] in which one assigns a single average excitation energy to the final nucleus, implying a single maximum photon energy $k_{\max}$. The transition strength is then evaluated at that excitation energy. The closure model has been criticized on theoretical grounds,[21] and indeed such calculations typically greatly overestimate the experimental photon yield for the ^{40}Ca test case.[16] A second difficulty with the closure model is that the extracted value of g_p is quite sensitive to the value of $k_{\max}$ used. Usually $k_{\max}$ is considered as a free parameter, and comparisons to data involve a simultaneous fit to g_p and $k_{\max}$.

There have been several recent attempts to calculate RMC while avoiding the closure approximation. Christillin[22] used a phenomenological nuclear excitation spectrum for ^{40}Ca, consisting of Lorentzian giant dipole and quadrupole components. The widths and relative strengths of the dipole and quadrupole terms were adjusted to reproduce existing photoabsorption and ordinary muon capture data. The predicted RMC branching ratio was lower than typical closure model results, bringing the theory into better agreement with experiment (assuming the PCAC value for g_p). A similar approach was adopted by Christillin and Gmitro[23] for ^{16}O. Account was taken of low-lying individual states in the ^{16}N final nucleus, in addition to the giant dipole and quadrupole terms.

A different approach is that taken by Gmitro *et al.*,[24] in which a microscopic calculation was made using shell-model wave functions. For ^{16}O n-particle, n-hole wave functions with $n = 0, 1, 2$ were used for the initial state, and the most important 1^- and 2^- T=1 levels were included for the final state. These wave functions were tested by comparing the predictions with existing data for electron scattering and radiative pion capture reactions, as well as for the ordinary muon capture rate. It was found that 2-particle, 2-hole correlations contributed significantly to both the OMC and RMC rates. RMC was also calculated for ^{40}Ca in this microscopic model; however, due to computational limitations only 1-particle,

1-hole wave functions were used. For ^{16}O and ^{40}Ca the predicted ratios of RMC/OMC were approximately a factor of 2 larger than those from the phenomenological calculations.[22,23] This was especially disturbing for ^{16}O, where the shell-model calculation would seem to be quite complete.

Recently, Roig and Navarro[25] have invoked SU(4) symmetry and applied sum-rule techniques to calculate RMC on ^{12}C, ^{16}O, and ^{40}Ca. The calculation was done within the impulse approximation, with sum rules calculated using a Hartree-Fock scheme for the target ground state. The branching ratios predicted for the latter two nuclides are substantially lower than those provided by both the phenomenological model and the microscopic model.

Attempts have been made to go beyond the impulse approximation and incorporate meson-exchange currents. Akhmedov, Tetereva, and Eramzhyan[26] found a reduction of the predicted RMC branching ratio of 10–12% for ^{40}Ca due to meson-exchange effects at the weak-interaction vertex. Meson-exchange effects at the electromagnetic vertex were included through constraints imposed by the electromagnetic continuity equation by Gmitro, Ovchinnikova, and Tetereva.[27] In this "modified impulse approximation" (MIA) approach, similar shell-model wave functions were used for ^{16}O and ^{40}Ca as in the earlier microscopic impulse approximation calculations.[24] The RMC branching ratios were reduced compared to the impulse approximation predictions, and for ^{40}Ca a reasonable agreement was found with the predictions using the phenomenological nuclear response. Results of the application of the MIA approach to ^{12}C have recently become available.[28] The theoretical situation for the targets measured in the present experiment is depicted in Fig. 1. A more detailed review of theoretical work on RMC can be found in Ref. 16.

III. EXPERIMENT

A. Experimental overview

The measurement of RMC requires a detection system with good efficiency and at least moderate resolution for photons in the energy range 50–100 MeV. Such a detector should also be insensitive to the large backgrounds of neutrons from muon capture and electrons from muon decay. It is also important to reject background photons from radiative pion capture (due to pions in the muon beam) and from cosmic-ray-induced events, and to ensure that the photons actually originate in the target. In this experiment, a system based on a time projection chamber (TPC) was used as a large solid-angle pair spectrometer to detect and track the e^+e^- pairs produced by the conversion of RMC photons in a Pb-scintillator converter package surrounding the target. Scintillation counters were used to count the beam particles stopping in the target, and a system of scintillators and multiwire proportional chambers provided the photon trigger. The spectrometer magnet was surrounded by external scintillators and drift chambers to identify cosmic-ray-induced events.

B. Muon and pion beams

The detector system was mounted at the end of a 10-m-long extension to the $M9$ stopped-π/μ channel at TRIUMF.[29] This channel views the production target (typically 10-cm-long beryllium) at 135° with respect

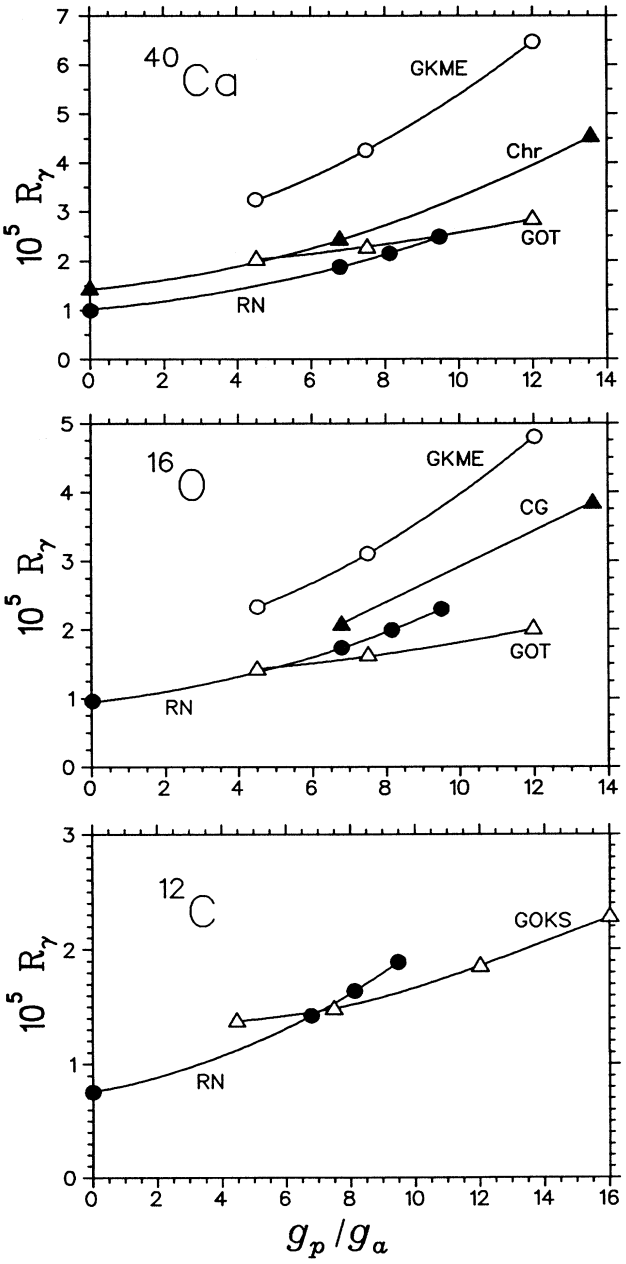

FIG. 1. Theoretical predictions for R_γ, the RMC partial branching ratio ($E_\gamma > 57$ MeV) as a function of g_p/g_a for ^{40}Ca, ^{16}O, and ^{12}C ("Chr," Ref. 22; "CG," Ref. 23; "GKME," Ref. 24; "RN," Ref. 25; "GOT," Ref. 27; "GOKS," Ref. 28).

to the incident beam, with a solid-angle acceptance of 25 msr. The primary beam consisted of 500 MeV protons with a typical current between 100 and 140 μA, a microstructure of 5-ns-long pulses every 43.3 ns, and a macroscopic duty factor of 100%.

The 73 MeV/c muon beam was produced by pion decays near the production target (cloud muons). After the 19-m drift to the TPC, the raw beam composition was $\pi/\mu \sim 1$ and $e/\mu \sim 10$. A radio-frequency particle separator[30] was used to suppress both the electron and pion content in the muon beam. The separated beam composition was measured to be $\pi/\mu \sim 10^{-3}$ and $e/\mu \sim 10^{-2}$. The negative muon flux was 5.0×10^5 s^{-1} with $\delta P/P$=10% incident on the beam counters with a spot size of 5×5 cm^2, which yielded typical stopping rates of 4.0×10^5 s^{-1} in the C and D_2O targets and 3.4×10^5 s^{-1} in the Ca target. A 73 MeV/c positive muon beam was also used for background studies.

Radiative pion capture reactions were measured on several targets, both to perform the calibration of the acceptance and resolution of the detection system, and to study pion-induced backgrounds. The momentum of the beam line was then tuned to 89 MeV/c to stop the pions in the targets, and the phase of the rf separator was tuned to transmit pions. At this momentum the time structure of the beam at the separator allows only a partial separation of the beam particles, and the beam composition was typically $\mu/\pi \sim 0.5$, $e/\pi \sim 1.7$. However, the three particle types all arrived at different times at the beam counters, so the pion stops in the target could be selected cleanly by a timing cut. The negative pion flux was varied to provide stopping rates in the targets between 1.0×10^3 and 4.0×10^5 s^{-1} to characterize the rate-dependent properties of the TPC.

C. Targets

Four different targets were used: calcium, oxygen, carbon, and polyethylene (CH_2). The calcium target consisted of a $10 \times 10 \times 1.9$ cm^3 block of natural calcium (96.97% ^{40}Ca), which had a thin layer of aluminum evaporated on all surfaces to reduce oxidation.

The oxygen target was approximately 500 ml of liquid D_2O (isotopically enriched to 99.96%) held in a polyethylene bag with walls 0.15 mm in thickness. The bag was roughly cylindrical with a radius of 7.6 cm and a length of about 3 cm. Water was used to provide sufficient muon stopping power, and D_2O was used rather than H_2O to reduce the background due to photons from the decay of π^0's produced by any π^-'s in the beam via the reaction $\pi^- p \rightarrow \pi^0 n$.[31,75] The fraction of muons that capture on the deuteron in the D_2O rather than on the oxygen is completely negligible. A small sample of data was taken with an identical target of H_2O.

The carbon target was a solid cylinder of graphite of radius 7.6 cm and length 1.9 cm. The CH_2 target, required for the calibration runs using radiative pion capture, was a solid cylinder of polyethylene of radius 6.25 cm and length 2.0 cm.

The target thicknesses were chosen to stop the muon or pion beam near the center of each target, which were placed in the geometrical center of the TPC.

D. Time projection chamber

The TRIUMF TPC has been described in detail elsewhere.[32–34] It is a large-volume, hexagonal drift chamber, located in parallel and uniform axial electric and magnetic fields. Ionization electrons created by charged particles that traverse the chamber volume drift in the electric field of $E = 250$ V cm^{-1} towards proportional wire chambers at the end caps of the detector.

The TPC was mounted inside a large-volume magnet which was obtained from the University of Chicago. For this experiment the magnet provided an axial field of 0.25 T with a measured uniformity of $\delta B/B < 0.3\%$ over the TPC volume. The TPC end caps each had 72 anode wires arranged in six sectors; behind each anode wire was a plane of segmented pads centered every 0.6 cm (636 pads/sector). As the drifting ionization electrons reached the end caps, segments of the track would pass through slots into these proportional wire chambers. Coordinates of the track in the x-y (transverse) plane were determined from the anode wire position and from the distribution of induced charge on the cathode pads. The (z) coordinate of the track was obtained from the electron drift time. Thus, up to 12 sets of (x,y,z) position coordinates were determined for each charged-particle track in the TPC, allowing a reconstruction of the helical trajectory. The cathode pad pulse heights also provided up to 12 independent samples of the particle's energy loss (dE/dx) in the chamber gas. All 144 anode wires were read out individually, but the cathode pads were multiplexed; each individual pad in a given sector was connected in parallel with the corresponding pad in each of the other sectors.

At high rates, the positive ions generated by the avalanche at the anode wires, if allowed to stream back into the drift volume, would seriously distort the electric fields in the drift region. To minimize this, a set of grid wires was installed at the entrance slot to each anode wire region.[34] These wires were normally biased at a potential that served to prevent both the ionization electrons from entering the proportional region and the positive ions from passing from the proportional region into the drift volume of the TPC. When the chamber was triggered the grid potential was pulsed to the "open" condition, which allowed only the passage of ionization electrons related to the trigger. This substantially lowered the rate on the anode wires, thereby reducing the positive ion effect as well as the aging effects in the chamber.

The various effects that determine the spatial resolution of the TPC have been studied previously.[33] The photon energy resolution was not limited by the spatial resolution of the TPC, but rather by energy loss and multiple scattering in the Pb converter.

E. Beam and trigger counters

With the exception of the photon converter package described below, the beam and trigger counters were identical to those used in previous experiments with the TPC, and more details are given elsewhere.[35] The scintillators used to count the incident beam particles and to define a stop in the target are shown in Fig. 2. They consisted of four beam counters B1–B4, each 10.4 cm (horizontal) by 15.8 cm (vertical). The first three scintillators were 0.63 cm thick. The last scintillator (B4) was 0.08 cm thick, to minimize the counting of false stops due to those low-energy particles which stopped in the last counter. These beam counters acted as live degraders to stop the incident muon beam in the target, and also aided in the rejection of background events due to pions in the beam. Also included upstream of the beam counters was a Pb collimator which was lined with scintillators (BV1–BV4) to minimize and reject any scattered beam. The entire beam counter assembly was recessed into the magnet so that the final beam counter was 35.0 cm upstream of the center of the TPC. A disk-shaped veto scintillator V (0.6 cm thick, 28 cm diameter) with an air light guide was located 14.5 cm downstream of the target to reject particles which passed through the target.

Three layers of scintillators surrounded the target. Each layer consisted of 18 individual counters 0.3 cm thick, together forming 18-sided polygons in cross section. Each counter was beveled at an 80° angle to minimize gaps between the counters. The assembly was oriented so that every three adjacent counters corresponded to one of the sectors of the hexagonal TPC. The inner two layers (IA1–IA18, IB1–IB18) served a dual purpose, both to complete the definition of an incident muon stop in the target, and to veto charged particles coming from the target. The IA layer had a 15.9 cm inner radius and 49.5 cm length and each counter was viewed by a separate photomultiplier tube. The IB layer had a 17.1 cm inner radius and 30.5 cm length; groups of three adjacent counters were connected to a single photomultiplier tube. A cylindrical sheet of Pb, 25.1 cm in length, was placed between the second (IB) and third (IC) layers of counters to convert photons from the target into e^+e^- pairs for detection in the TPC. On different runs, two different Pb converters were used: 0.6 mm thick (^{40}Ca, ^{12}C targets) and 1.0 mm thick (^{40}Ca, ^{16}O, and ^{12}C targets). The final layer of counters (IC1–IC18) with an inner radius of 18.4 cm and a length of 27.9 cm was used to detect the charged leptons from converted photons. Each of these counters was viewed by a single photomultiplier tube. The segmentation of these counters allowed the rejection of backgrounds through the ability to look for a valid spatial trigger pattern, and also kept the singles rate in each counter low.

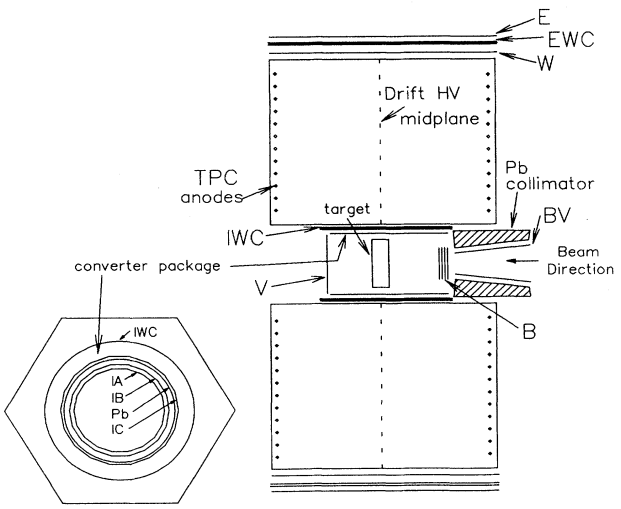

FIG. 2. Schematic cross section of the TPC, beam scintillators (B), the beam-veto scintillators (BV,V), and trigger counters (IA,IB,IC,IWC,W,EWC,E). The detail in the lower left shows a cross section of the converter package. Not to scale.

The converter package was surrounded by a cylindrical wire chamber (IWC) of inner radius 9.9 cm, outer radius 12.0 cm, and length 47.0 cm. The chamber had 192 anode wires strung axially at a spacing of 0.358 cm, and two layers of 128 helical cathode ribbons, inside and outside the anodes. The cathodes were of opposite pitch, each completing a rotation of 90° along the length of the chamber; the combination of the anode and cathode information gave both the axial and azimuthal coordinates of a charged particle passing through the IWC.

Surrounding the TPC were outer trigger counters made up of 6 sets of planar counters, each covering a sector of the TPC. Each set consisted of three counters: a wire chamber (EWC1–EWC6) sandwiched between two scintillators, W1–W6 and E1–E6. Closest to the TPC were the counters W1–W6 which were 80 cm long in the axial direction, 61.5 cm wide, and 1.3 cm thick; these were read out via BBQ wave-shifter bars. The EWC wire chambers were not used in the present experiment. The final layer of scintillators E1–E6, were 80 cm long, 67 cm wide, and 0.64 cm thick.

Surrounding the magnet were counters to veto cosmic-ray-induced events. These consisted of 12 large-area drift chambers of various sizes and 6 groups of large scintillators. The top and all four sides of the magnet were covered by a double layer of drift chambers and a single layer of scintillators.

F. Trigger

The first-level trigger defined a stop in the target: STOP$\equiv B1 \cdot B2 \cdot B3 \cdot B4 \cdot \overline{V + \Sigma BV} \cdot \overline{\Sigma IA + \Sigma IB} \cdot RF$, where RF was a timing signal relative to the cyclotron rf to select muons or pions as appropriate. A live-time gate LT, whose width was set appropriate to the μ^--capture lifetime in each target, was generated by STOP if no blanking signal was present. Photon triggers were accepted during the LT gate, which was 4.0 μs long for the ^{12}C and ^{16}O targets, 950 ns long for the ^{40}Ca target, and

30 ns long for pion calibration runs.[36] The blanking signal included computer-busy, rf separator fault, magnetic-field fault, chamber high-voltage fault conditions, etc. The LT gate was bypassed for cosmic-ray background data taking.

The photon trigger required: (1) LT signal present; (2) Absence of hits in any IA or IB veto scintillator; (3) $IC_i \cdot IWC_i \cdot (W_j + E_j) \cdot (W_k + E_k)$, where $j \neq k$ and $j,k = i-1, i$ or $i+1$ and $1 \leq i,j,k \leq 6$ (cyclic) are the sector numbers of the hexagonal TPC. This required that at least one of the outer counters (E, W) had fired in at least two of the three outer sectors corresponding to the inner counters (IC, IWC) hit; (4) ≥ 6 TPC anode wire hits.

The typical trigger rate was 4–10 s^{-1} during RMC data taking. Details on the trigger logic are given elsewhere.[35,37]

G. Data acquisition

The data acquisition system has been described elsewhere.[38] It consisted of a seven-crate CAMAC acquisition system, external memory, and PDP 11/34 and VAX 11/750 computers. The PDP handled the task of reading the data from CAMAC and transferring it to tape, updated various histograms of the raw data, and performed several basic monitoring and control processes. It also passed a fraction of the events to the VAX via DECNET for on-line analysis.

The analog pulse heights on each of the 144 anode wires and the 636 12-fold multiplexed cathode pads were digitized using the LeCroy 2280 CAMAC ADC system. The analog signals from all 144 TPC anodes were also discriminated and sent to bit registers to provide the pattern of hits in the chamber. The time information from the anode wires was multiplexed by sector, and digitized in 12 TDC channels. Therefore, if two tracks fired a given anode wire, only the arrival time of the earliest ionization to reach the anode wire was digitized. Information from the beam, trigger, and cosmic-ray counters was also digitized by CAMAC modules and written to tape for each event. The typical event size was 700 words.

A final level of software-based trigger was provided by the PDP. Events were rejected if the number of words of data from the 2280 ADC's was too small to be a valid photon event, and also if the number of hits on the cathode pads was too small. These cuts were able to reduce the rate of events written to tape by another factor of 50–60 % , with essentially no loss of good data (< 2% typically). The data-acquisition system was able to handle the maximum trigger rate during the RMC data taking of ≤ 10 s^{-1} with a dead time of $\leq 20\%$.

IV. DATA ANALYSIS

A. Track reconstruction

The track reconstruction algorithms used in this experiment were only slightly different from those used previously for the analysis of single-track data obtained with the TPC,[35] and consequently they will not be discussed here. Small modifications were made to these algorithms to enhance the reconstruction efficiency for photons; these are described in detail in Ref. 37.

B. Cuts

After the track reconstruction, various cuts were applied to the data to reject background events and poorly-fit tracks. These cuts were based upon the characteristics of the fitted tracks in the TPC as well as information from the trigger counters and other components of the detection system. The determination of the efficiency of each cut was made using both the pion calibration data, and also Monte Carlo simulated data. With one exception, identical cuts were used in the analysis of RMC data, pion calibration data, and Monte Carlo simulated data, so that the acceptance determined from the calibration data represented the actual acceptance for RMC data. The exception was the prompt cut, which was used to reject pion-induced background, and so was inappropriate for the pion calibration data.

The cuts applied to the data are summarized as follows:

(1) Track fitting: Maximum number of TPC wires missing data; maximum number of TPC hits not related to the pair; maximum number of points shared by the two tracks; and a quality-of-fit cut based on the χ^2 for the track fit procedure.

(2) Geometry: Maximum opening angle of the pair; maximum difference in both azimuthal angle (ϕ) and axial position (z) between the intersections of the tracks in the pair with the converter; maximum deviation in both ϕ and z between the track position determined by the IWC and the projection of the fitted track; maximum radial distance of closest approach of reconstructed photon to target center; maximum distance in z between the track intersection with the converter and the target.

(3) Trigger: Correct trigger counter pattern corresponding to fitted tracks.

(4) dE/dx: Maximum median energy loss measured in the TPC for each track.

(5) Cosmic-ray veto: Rejection of events with various combinations of cosmic-ray veto drift chambers and scintillators firing in coincidence with the event.

(6) Prompt (pion) veto: Rejection of any event with two or more beam counters firing in prompt (30 ns) coincidence with the event.

A typical event passing all cuts is depicted in Fig. 3.

C. Response function

The photon response function was determined using the GEANT Monte Carlo simulation program.[39] Monoenergetic photons were generated at 10 MeV intervals between 40 and 150 MeV; typically 4×10^5 photons were generated at each energy. The initial locations of the photons were sampled from a realistic stopping distri-

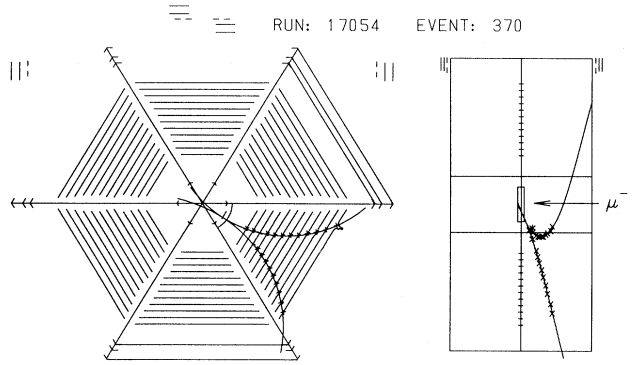

FIG. 3. Pictorial representation of a typical reconstructed photon event that satisfied all the cuts.

bution in the target. The simulated events were then analyzed like actual data, and the reconstructed photon energy spectra were fitted to a response function of the following form:

$$D(E_\gamma, E) = A \exp\left[-\frac{1}{2\sigma_0^2}(E - E_0)^2\right] \quad \text{for } E_1 < E < E_2, \tag{2}$$

$$D(E_\gamma, E) = B \exp\left[-\frac{1}{2\sigma_1}(E_1 - E)\right] \quad \text{for } E < E_1, \tag{3}$$

$$D(E_\gamma, E) = C \exp\left[-\frac{1}{2\sigma_2}(E - E_2)\right] \quad \text{for } E > E_2, \tag{4}$$

where

$$E_1 = E_0 - \frac{\sigma_0^2}{\sigma_1}, \tag{5}$$

$$E_2 = E_0 + \frac{\sigma_0^2}{\sigma_2}, \tag{6}$$

and

$$B = A \exp\left(-\frac{\sigma_0^2}{2\sigma_1^2}\right), \tag{7}$$

$$C = A \exp\left(-\frac{\sigma_0^2}{2\sigma_2^2}\right), \tag{8}$$

and A, E_0, σ_0, σ_1, and σ_2, are free parameters. E_γ is the actual photon energy and E is the reconstructed energy. This function is essentially a Gaussian with high- and low-energy tails which gave a reasonable representation of the line shape. For clarity, the function is not given in normalized form. The parameters E_0, σ_0, σ_1, and σ_2 were then fitted to polynomial functions of E_γ, e.g.,

$$\sigma_0 = P_0 + P_1 E_\gamma + P_2 E_\gamma^2 + P_3 E_\gamma^3 \quad . \tag{9}$$

The values of the coefficients P_0, P_1, P_2, and P_3 for each fit are given in Table I. Figure 4 shows the energy spectrum for 70 MeV photons with the fit superimposed. The chosen function parametrizes the GEANT results well, except for the details of the extreme high-energy "tail" of the line shape. This tail will be seen to be rather important, and will be discussed in more detail in the next section. With the detector response function parametrized as above, the Monte Carlo prediction for the observed spectrum for any given theoretical input spectrum was easily produced analytically, thereby avoiding the necessity of running Monte Carlo simulations for each input spectrum.

The final parameter A is related to the photon acceptance. Figure 5 shows the photon acceptance as a function of photon energy for the two converter thicknesses. The absolute normalization of the acceptance given is a "zero-rate" value. The energy dependence of the acceptance was parametrized by the function

$$\epsilon\Omega = A_0 \left\{ \mathrm{erf}\left[\frac{(E_\gamma - A_1)}{A_2}\right] - \mathrm{erf}\left[\frac{(A_1 - E_\gamma)}{A_2}\right] \right\} + A_3 \quad , \tag{10}$$

TABLE I. Coefficients of polynomial fits to the energy dependence of the photon response function parameters.

Converter (mm)	Parameter	P_0 (MeV)	P_1	P_2 $(\mathrm{MeV})^{-1}$	P_3 $(\mathrm{MeV})^{-2}$
0.6	E_0	−7.548	1.1403	-1.028×10^{-3}	
	σ_0	−3.365	0.2026	-2.216×10^{-3}	1.188×10^{-5}
	σ_1	6.402	−0.2560	3.697×10^{-3}	-1.389×10^{-5}
	σ_2	1.983	−0.0641	9.606×10^{-4}	1.880×10^{-7}
1.0	E_0	−9.823	1.1381	-1.013×10^{-3}	
	σ_0	5.186	0.1900	3.240×10^{-3}	-9.608×10^{-3}
	σ_1	−11.786	0.5410	-7.128×10^{-3}	-3.715×10^{-5}
	σ_2	−1.700	0.1312	-1.604×10^{-3}	1.001×10^{-6}

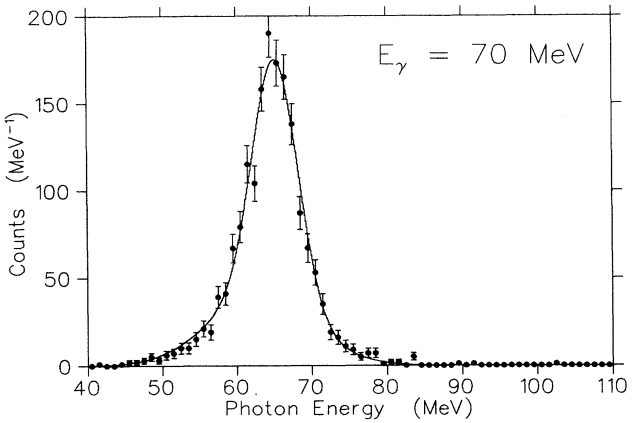

FIG. 4. Monte Carlo simulation of the photon energy spectrum for 70 MeV photons using a 1.0-mm-thick converter (points), and the parametrization using the detector response function described in the text (solid line).

where the fitted values of the coefficients A_0, A_1, A_2, and A_3 are given in Table II. This functional form was chosen for convenience.

The detector response function produced using GEANT was checked by comparing the predictions to experimental data taken during the pion calibration runs. For both radiative pion capture on ^{12}C, and the radiative pion capture and pion charge-exchange reactions on the proton, high-quality data with good energy resolution are available. These spectra were folded with the detector response function as parametrized above, and compared with the data. Figure 6 shows this comparison for radiative pion capture on ^{12}C, using the data of Perroud *et al.*[40] for the input spectrum.

The data for the π^- p reaction were obtained by subtracting a suitably normalized spectrum of ^{12}C(π^-,γ) from CH_2(π^-,γ). The π^- p reaction at rest has two branches:[41]

$$\pi^- p \rightarrow \pi^0 n \quad (60.4\%), \tag{11}$$

TABLE II. Coefficients of the fit to the energy dependence of the photon acceptance

Converter (mm)	A_0	A_1 (MeV)	A_2 (MeV)	A_3
0.6	1.056×10^{-3}	80.22	24.05	2.033×10^{-3}
1.0	1.583×10^{-3}	77.88	28.32	2.792×10^{-3}

$$\pi^- p \rightarrow \gamma\ n \quad (39.6\%), \tag{12}$$

where the radiative capture gamma ray (Eq. 12) has an energy of 129.4 MeV, and the π^0 nearly always decays into two photons (98.8% branch) providing a continuous photon energy spectrum between 54.9 and 83.0 MeV. Figure 7 shows the π^- p spectrum compared with the Monte Carlo prediction. The effect of the slightly different photon interaction probabilities in the C and CH_2 has been accounted for in the Monte Carlo results. The agreement here is generally good, except at the upper end of the π^0 portion of the spectrum. This is due in part to the necessary subtraction of the ^{12}C(π^-,γ) spectrum but also to inaccuracies in the simulation of the low-energy tail of the response for the 129 MeV photon. The detector resolution was quite poor for photons with energies as large as 129 MeV. For these photon energies the tracks in the TPC have very large radii of curvature leading to poorer momentum resolution. The RMC spectrum endpoint ($\sim$ 100 MeV) is well below these energies. At the low-energy end of the π^0 spectrum where one has more confidence in the accuracy of the Monte Carlo, the data are well reproduced by GEANT. Because only the high-energy portion (above 57 MeV) of the RMC photon spectrum is used in the calculation of the partial branching ratio, a systematic error due to the energy calibration at 57 MeV must be assigned. An energy calibration error of $\pm$400 keV was estimated from comparisons between GEANT and the data for the ^{12}C(π^-,γ) spectrum, the low-energy end of the $\pi^0 \rightarrow \gamma\gamma$ spectrum, and the spectrum of bremsstrahlung photons from positrons from μ^+ decay.

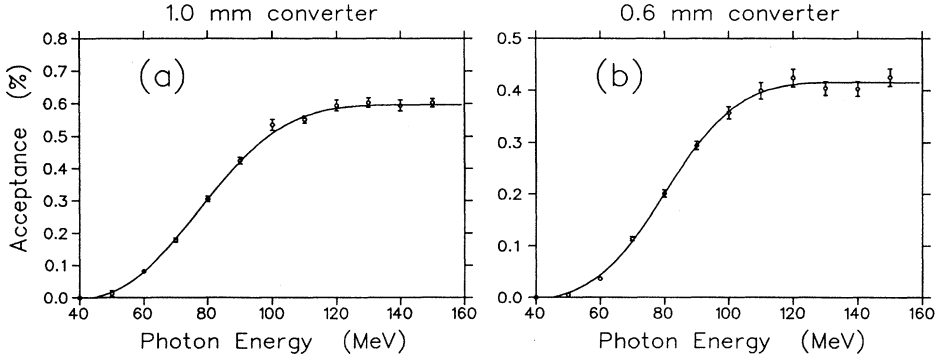

FIG. 5. Monte Carlo simulation of the photon acceptance as a function of photon energy, for (a) 1.0-mm-thick converter and (b) 0.6-mm-thick converter. The solid lines are the fits using the parameters given in Table III.

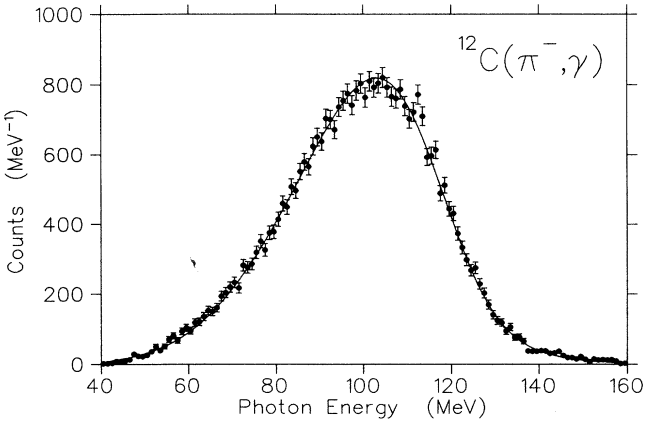

FIG. 6. Photon energy spectrum from radiative pion capture on ^{12}C using the 1.0-mm converter. The solid line is a Monte Carlo simulation for this spectrum. The input photon energy spectrum used in the Monte Carlo simulation was taken from Perroud *et al.*[40]

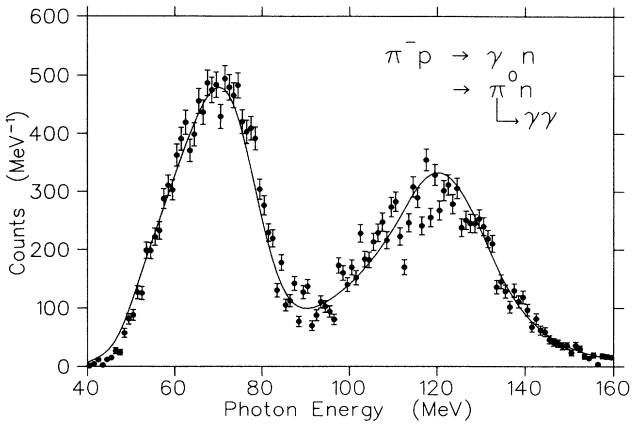

FIG. 7. Photon energy spectrum from radiative pion capture and charge exchange on hydrogen using the 1.0-mm converter, obtained from a subtraction of spectra from CH_2 and C. The solid line is a Monte Carlo simulation for this spectrum.

D. Backgrounds

1. *Bremsstrahlung*

Some fraction of the μ^-'s stopping in the target will not undergo nuclear capture, but will decay instead. These muon decay events can produce photons either via bremsstrahlung of the decay electrons in the target or surroundings (external bremsstrahlung), or via radiative muon decay (internal bremsstrahlung). For the decay of the free muon, neither of these processes can produce photons of energy greater than 53 MeV (the end point of the electron spectrum from muon decay). Below this energy, however, there is a copious background of photons from these processes, especially for light nuclei, where the majority of μ^-'s in the target decay rather than capture. This background limits measurements of RMC to that portion of the spectrum above a lower limit, typically 57 MeV to allow for finite detector resolution.

Bremsstrahlung photons can appear above 53 MeV in the experimental spectrum due to (a) the high-energy tail in the detector response function and (b) distortions in the decay-electron spectrum due to the fact that the μ^- is bound, not free. In the present experiment the first effect dominated. Rather than relying on the Monte Carlo to predict the extreme high-energy tail of the detector response function it was determined experimentally using a stopping μ^+ beam. A μ^+ will undergo internal and external bremsstrahlung the same as a μ^-; however, it will not undergo nuclear capture. The additional processes of positron annihilation-in-flight and Bhabha scattering were found (by Monte Carlo using GEANT) not to affect significantly the shape of the photon spectrum in the region of interest. Figure 8 shows the summed experimental (μ^+,γ) spectrum using both ^{12}C and D_2O targets.

The observed high-energy tail, defined as the fraction of the bremsstrahlung events observed above 57 MeV, was $(2.1 \pm 0.3)\%$. The error is purely statistical. By normalizing to the number of bremsstrahlung events below 57 MeV in the μ^- data (after subtracting the contribution from RMC), the contribution of the high-energy tail to the observed spectrum above 57 MeV can be estimated. Table III gives these estimates. For the ^{12}C and ^{16}O cases, the tail calculated from the μ^+ spectrum alone has been used; as discussed below, the differences between the *free* decay bremsstrahlung spectrum (the μ^+ spectrum) and the *bound* muon decay spectra for these targets are negligible. For ^{40}Ca a correction to the contribution determined from the μ^+ data has been added to account for the muon-binding effects. This gives an *effective* high-energy tail of $2.1\% + 1.1\% = 3.2 \pm 0.4\%$ for ^{40}Ca.

For a bound μ^-, a small portion of the decay spectrum extends above 53 MeV. To calculate the effect of this for

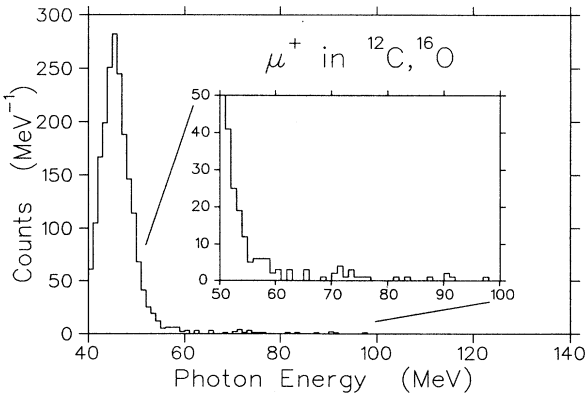

FIG. 8. Summed photon energy spectra from μ^+ stopping in ^{16}O and ^{12}C. The events above 53 MeV are due to the high-energy tail in the detector response function.

TABLE III. Backgrounds to the RMC spectrum. All contributions are given in terms of % of the RMC spectrum ($E_\gamma > 57$ MeV).

Target	Converter (mm)	Bremsstrahlung	RMC in scintillators	Cosmic rays	(π^-, γ)
^{12}C	0.6	17 ± 2	6.1 ± 1.8	1.6 ± 0.2	0.04 ± 0.01
	1.0	14 ± 2	6.1 ± 1.8	1.5 ± 0.2	0.90 ± 0.14
^{16}O	1.0	6.2 ± 0.9	2.5 ± 0.8	1.2 ± 0.1	0.06 ± 0.01
^{40}Ca	0.6	0.50 ± 0.07	0.5 ± 0.2	0.20 ± 0.03	< 0.01
	1.0	0.30 ± 0.04	0.5 ± 0.2	0.18 ± 0.02	< 0.01

the present experiment, the Monte Carlo code GEANT was used to simulate bremsstrahlung photon spectra for each of the targets. The decay-electron spectrum was taken from the analytic expression derived by Hänggi *et al.*[42] [Eq. (13) of Ref. 42, corrected according to Herzog and Alder[43]]. The internal bremsstrahlung process was of comparable importance to external bremsstrahlung for the targets used, and it was modeled in the same way, using the photon spectrum given in Ref. 44. The sum of the external and internal bremsstrahlung spectra was then compared with the observed spectra, after the contribution from RMC was subtracted. Figure 9 shows this comparison for ^{12}C, where a simple polynomial form has been used for the RMC spectrum. The ^{16}O case is similar. For ^{40}Ca the RMC signal overwhelms the bremsstrahlung background, and no such comparison was attempted. The spectra generated for each target could then be used to predict the bremsstrahlung contribution above 57 MeV. For both ^{12}C and ^{16}O the contribution to the photon spectrum above 57 MeV was found to be identical within error to that from free μ^+ decay; i.e., the μ^- binding effects were negligible.

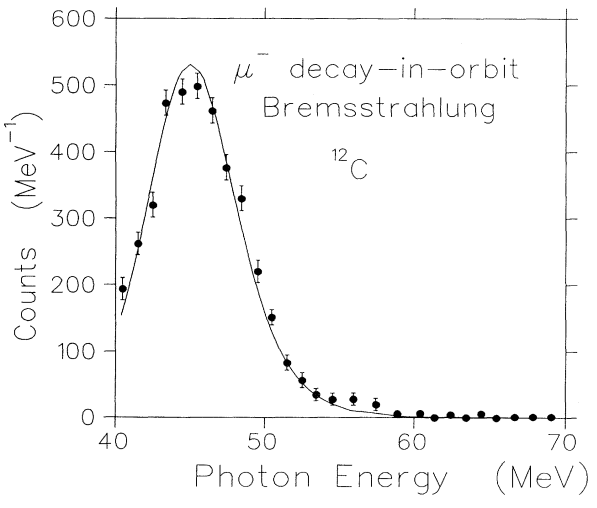

FIG. 9. Photon energy spectrum due to bremsstrahlung of decay electrons from muons bound in ^{12}C. The RMC signal has been subtracted using a simple polynomial form for the theoretical RMC spectrum. The solid line is a Monte Carlo simulation.

Since μ^+ data were taken only using the 1.0-mm converter, the assumption has been made that the high-energy tail was the same as for the 0.6-mm converter, since the high-energy tail was primarily due to the track-fitting and not due to interactions in the Pb.

For the final analysis, the normalized μ^+ data were subtracted from the μ^- spectrum to yield the final RMC spectrum. In principle, this would also allow the RMC data below 57 MeV to be used to obtain the branching ratios; however, this was not done, because the statistical gain was more than offset by the added uncertainty due to the subtraction of a large background. There are also minor differences between the shapes of the μ^+ and μ^- bremsstrahlung spectra below 57 MeV.

2. *Muon stops outside the target*

Background from RMC of muons that stopped in the scintillators surrounding the target was potentially a serious problem, especially for the ^{16}O and ^{12}C targets, where the RMC rate from the target material is small. The fraction of the muon beam that scattered into the scintillators surrounding the target was measured by CAMAC scalers. The contribution to the RMC spectrum from this background was then estimated using the measured RMC rate on carbon (muon capture on the hydrogen in the scintillator is negligible). This was then corrected for the geometrical reduction in acceptance for photons originating in the scintillators (determined by Monte Carlo) and the probability of the LT gate already being open from a previous μ stop. The resulting estimated background contribution to the RMC signal from each target is given in Table III.

These background estimates were confirmed by examining the time distribution of the photon events. Photons from RMC in the target surroundings would be uncorrelated in time with the LT gate. The background contribution was extracted by fitting the time distribution of the photon events (relative to the time of the LT gate) and determining the component that does not exhibit the correct muon lifetime in the given target. The distortion in the time distributions due to pileup of the incident muons

on the time distributions was calculated by Monte Carlo. The time distribution of the good photon events was fitted to a sum of two exponentials, one with the apparent lifetime appropriate for the target, and one with the apparent lifetime of a time-independent background at the relevant muon stopping rate. The amplitudes of the two exponentials were free parameters in the fit. Figure 10 shows the fit for the ^{16}O data for all photon energies. In all cases the background extracted from the photon time distribution was consistent with the estimates given in Table III.

3. Cosmic rays

More than 850 hours of cosmic-ray background data were collected, both between and after various data-taking runs, in order to determine the background due to photons from electromagnetic showers induced by cosmic rays. A small rate of real photons was observed (3×10^{-4} s^{-1}) in the cosmic-ray background data. In most of these events, one or more of the cosmic-ray drift chambers or scintillators had fired in prompt coincidence with the event. A set of cosmic-ray cuts was developed, based upon various combinations of cosmic-ray and trigger counters having fired, which eliminated all but a few events. The energy spectrum of these remaining events is shown in Fig. 11. The rate for cosmic-ray photons in the energy range of the RMC spectrum (57 to 100 MeV) was 0.8 ± 0.1 events/day. The number of cosmic-ray photons in the RMC spectrum was estimated from this rate after correcting for the dead time. Table III gives the results for the three targets. Since almost all the cosmic-ray background data were obtained with the 1.0-mm converter, the background rate for the data taken with the 0.6-mm converter was estimated by scaling by the relative photon acceptances for the two converter thicknesses. In each case the cosmic-ray background was $\leq 2\%$ of the RMC signal.

4. Pion capture

The branching ratio for radiative pion capture is typically $\sim 2 \times 10^{-2}$,[45] several orders of magnitude larger than the expected signal from RMC ($\sim 10^{-5}$ per captured muon). Therefore, even a very small pion contamination in the beam could cause a photon background larger than the RMC signal.

This potential background was reduced in several ways. The first stage was the rf separator, which reduced the π/μ ratio in the beam to approximately 10^{-3}. Secondly, due to the shorter range of the pions, the majority of pions remaining downstream of the separator stopped in the beam counters in front of the target. The final stage of pion reduction was achieved by rejecting any photon event in prompt coincidence with an incident beam particle. A bit register was set if any two of the four beam counters fired in coincidence with a photon trigger, and events with this "prompt bit" set were rejected in the analysis. Figure 12 shows the spectra of all such prompt events for the three targets; in the oxygen and carbon cases, one can clearly see a radiative pion capture spectrum. There are also some events that are RMC and bremsstrahlung events that were in random coincidence with an incident beam particle. From the observed number of radiative pion capture events in the prompt spectrum, the pion content of the beam reaching the target was determined to be typically 1.5×10^{-5}. The larger radiative pion capture signal seen in the carbon data (see Fig. 12) is due to a subset of the data (about 20% of the total) where the pion content of the beam was an order of magnitude larger than normal, due to the phase of the rf separator being improperly set.

The pion-rejection efficiency of the prompt cut was measured separately by tuning to a pion beam, and determining the fraction of radiative pion capture events

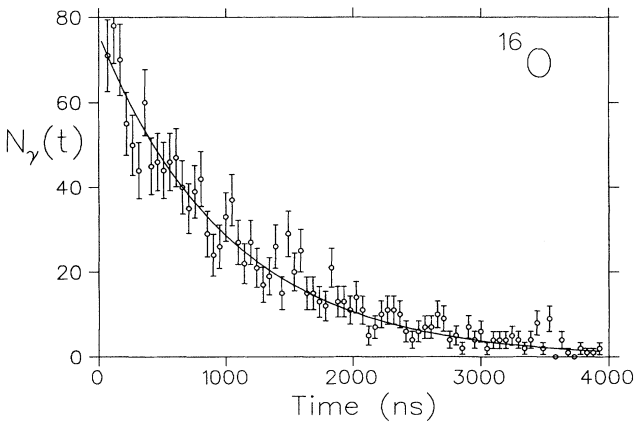

FIG. 10. Time distribution of photon events from the ^{16}O target, relative to the last previous muon stop (LT gate). All photon energies are included. The solid curve is the result of a fit to the effective muon lifetime in ^{16}O, i.e., with account taken of pileup of the incident muons.

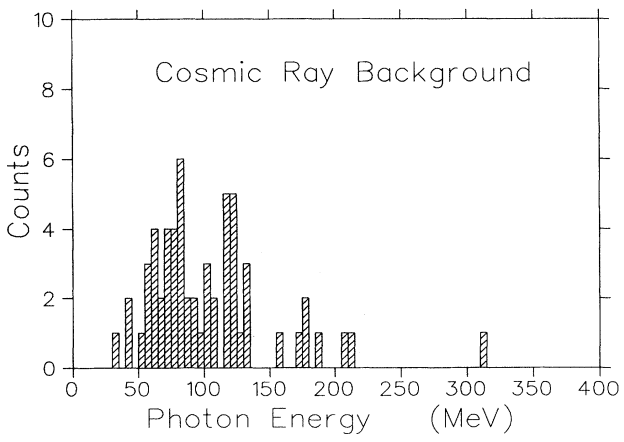

FIG. 11. Photon energy spectrum from cosmic-ray background, after all cuts imposed, for the 1.0-mm converter.

that did not have the prompt bit set. This was found to be (0.61±0.10)%. The number of pion-induced events remaining in the RMC spectrum after the prompt cut could then be determined by applying this fraction to the number of radiative pion capture events seen in the prompt spectrum; the results are given in Table III. The background was $\leq$ 1% of the RMC signal in all cases. The overall suppression factor of the pion-induced background was typically 10^7. A comparison of the non-prompt RMC spectra with the radiative pion capture spectra clearly shows the almost complete absence of pion-induced photons after the prompt cut.

5. Other backgrounds

In addition to the background processes discussed above, other backgrounds were also considered. One of these is the copious flux of neutrons from ordinary muon capture. This has posed serious troubles for some previous RMC measurements using NaI detectors.[46,47] For ^{40}Ca the branching ratio for high-energy neutrons is an order of magnitude larger than that for RMC photons,[48] and so very efficient neutron discrimination is required. This background was eliminated in the present experiment, as the TPC is completely insensitive to neutrons. Similarly, muons scattered into the TPC, or protons from μ^- capture in the target or (n,p) reactions in the target area, were easily rejected by their large energy loss in the TPC (i.e., by the dE/dx cut). A final possible background is bremsstrahlung due to the electrons that comprise ~1% of the muon beam. These were rejected along with the radiative pion capture photons by the prompt cut, and contributed << 1% to the signal.

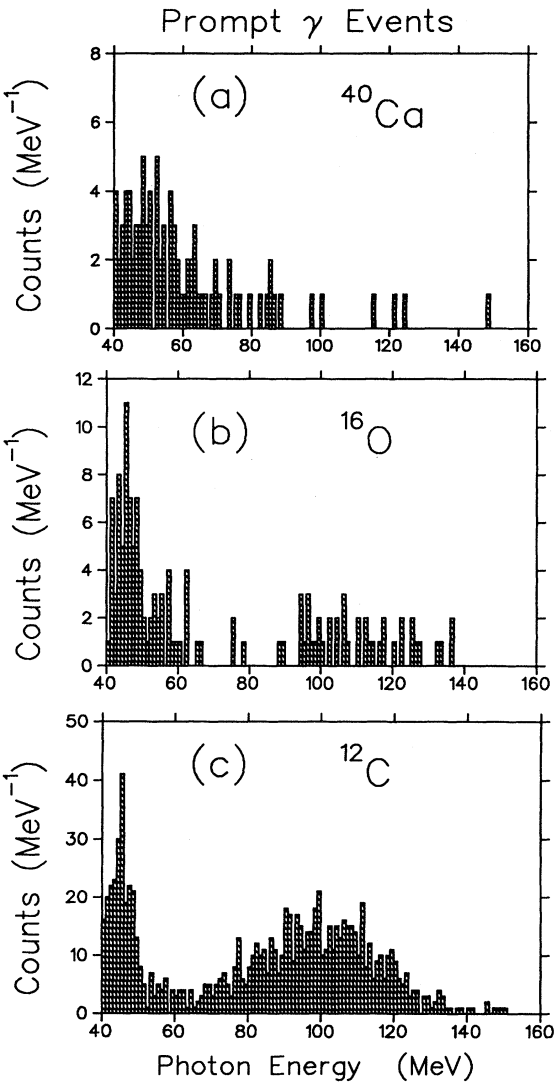

FIG. 12. Photon energy spectrum for prompt events from (a) ^{40}Ca, (b) ^{16}O, and (c) ^{12}C using the 1.0-mm converter. The events above ~ 80 MeV are due to radiative pion capture.

E. Rate dependence

The photon acceptance of the detector was found to depend strongly on the particle flux in the TPC, or equivalently on the rate of particles stopping in the target. This is seen in Fig. 13, which shows the relative acceptance measured using $^{12}C(\pi^-,\gamma)$ and $CH_2(\pi^-,\gamma)$ versus the singles rate of one of the TPC anode wires. A series of tests ruled out the possibility that the observed decrease in acceptance was due to dead-time effects, miscounting of the incident beam, changes in the beam profile or problems in the trigger electronics.[37] This rate effect was measured to high precision using (π^-,γ) and was found to be independent of the target used. A series of (μ^-,γ) runs with the ^{40}Ca target verified that the (μ^-,γ) rate effect was identical to that found using (π^-,γ). A similar

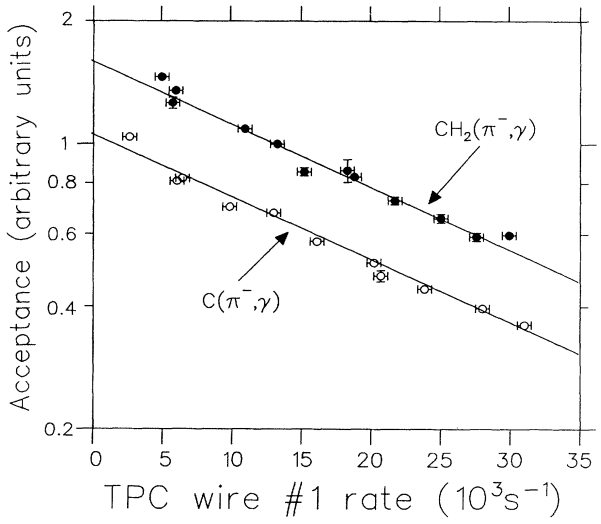

FIG. 13. Rate dependence of the photon acceptance, shown as a function of the rate of firing of the innermost TPC anode wire (wire No. 1), as measured using radiative pion capture. The lines are least-squares fits to simple exponentials. The RMC data were obtained at rates of typically 20×10^3 s^{-1}.

rate dependence was found for single-track data obtained from tests using muon-decay electrons, (π^+, π^+) elastic scattering and also positrons from the decay $\pi^+ \rightarrow e^+\nu$.

This rate dependence was attributed to positive-ion space-charge effects in the proportional wire regions of the TPC. The amplitudes of the signals from the TPC cathode pads (and anode wires) were found to decrease as the rate was increased. At high rates the buildup of positive ions caused a reduction in the electric field near the anode wires of the TPC, causing a reduction in gain. This in turn reduced the amplitude of the induced signals on the cathode pads, causing some of them to fall below threshold. Consequently, fewer valid (x, y) points were available for the track reconstruction, thereby reducing the event reconstruction efficiency and thus causing a loss in acceptance. Such positive-ion effects have been reviewed by Sauli;[49] a typical critical wire rate for gain reduction is 10^9 electrons s^{-1} mm^{-1}. The TPC anode wire rate was dominated by primary particles entering the proportional region (these are unaffected by the gated-grid system[34] which prevented the drift electrons from the chamber volume from entering the proportional region except for valid triggers). A minimum-ionizing particle crossing the proportional region generates ~ 300 electron-ion pairs. At the gain of the TPC (5×10^4) the critical rate thus corresponds to a wire rate of 7×10^3 s^{-1}, which is of the same order as the wire rates in the present experiment. Therefore positive-ion effects in the proportional region are a plausible explanation for the observed loss of amplitude. There was no evidence for a significant positive-ion effect in the drift volume. The problem was exacerbated by the ageing of the chamber; by the end of the experiment the accumulated charge on the inner wires of the TPC was on the order of 10^{16} electrons mm^{-1}.

Confirmation that the reduction in cathode-pad amplitude was the cause of the rate dependence was obtained by reducing the cathode-pad amplitude in the Monte Carlo simulation in the same manner as observed in the data. An identical reduction in the number of points per track and hence the acceptance was found as observed in the data (see Fig. 14). All other experimental variables simulated via Monte Carlo were in agreement with the data once this pad amplitude effect was incorporated. This provided one of the two methods used to correct for the rate dependence: The RMC data were normalized to Monte Carlo data with equivalent pad amplitudes. The second method was to use the acceptance as determined from (π^-, γ) data taken at the same TPC wire rates as the RMC data. The two methods yielded consistent results.

F. Photon acceptance and (π^-, γ) results

The absolute photon acceptance was determined by normalizing to the well-known branching ratio for radiative pion capture on ^{12}C. The weighted average of three, mutually consistent, measurements of this branching ratio is $(1.83 \pm 0.06)\%$.[40,45] High-statistics data were obtained for $^{12}C(\pi^-,\gamma)$ over a wide range of beam rates. The measured absolute acceptance agreed to within 7% with that predicted using the GEANT simulation.

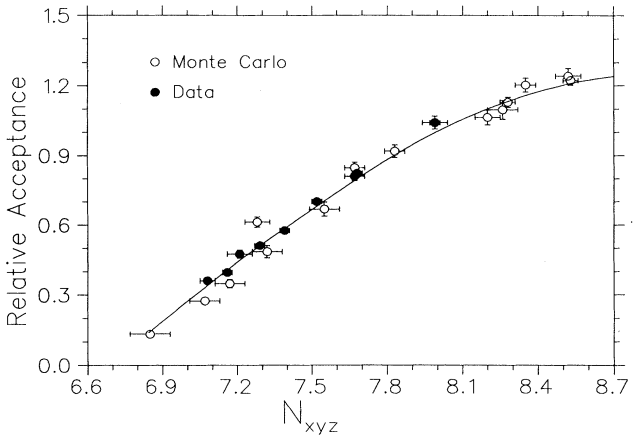

FIG. 14. Dependence of the photon acceptance on the number of points per fitted track (N_{xyz}), compared to Monte Carlo prediction. The solid circles are the data and the open circles are the Monte Carlo results. The solid curve is a spline fit to the Monte Carlo.

The normalization to the $^{12}C(\pi^-,\gamma)$ data includes small corrections for pion decay-in-flight, $(4.4 \pm 0.6)\%$, pileup in the counting of the incident pions ($< 1.2\%$ at the highest beam rate used) as well as the effect of vetoing due to the random firing of an IA or IB veto counter. The error assigned to the absolute acceptance also includes a factor due to photon absorption in the target, which was estimated from GEANT using a wide range of stopping distributions within the target. The factors contributing to the uncertainty in the absolute normalization are listed in Table IV.

The (π^-,γ) spectrum from hydrogen, obtained by subtracting (π^-,γ) spectra from CH_2 and C, was not used for the normalization of the acceptance. This is because one needs to know $W(CH_2)$, the fraction of pions that capture on the hydrogen in CH_2, which is not accurately known. A weighted average of five measurements[45,50–53] gives $W(CH_2)=(1.26\pm0.12)\%$ [the mutual agreement of these data is poor, and so the error in $W(CH_2)$ has been scaled up by the square root of the reduced χ^2 to reflect this]. The value of $W(CH_2)$ determined in this experiment as well as the measured radiative pion capture branching ratios for ^{40}Ca and ^{16}O are in good agreement with previous data (see Table V) using the normalization chosen.

G. Branching-ratio calculation

The observed photon energy spectrum $dN_\gamma(E)/dE$ from RMC is related to the physical photon energy spectrum $d\Lambda(E_\gamma)/dE_\gamma$ by

TABLE IV. Contributions to the error in the absolute normalization of the photon acceptance ($\epsilon\Omega$). The errors have been added in quadrature to give the total error.

(π^-,γ) Branching-ratio error	3.4 %
Pion decay in flight	0.6 %
Photon absorption in target	2.0 %
Rate effect	3.6 %
Statistics	0.7 %
Total error	5.4 %

$$\frac{dN_\gamma(E)}{dE} = N_\mu f_{\rm cap} \int dE_\gamma \, D(E_\gamma, E) \, \epsilon\Omega(E_\gamma) \, \frac{d\Lambda(E_\gamma)}{dE_\gamma} \quad , \tag{13}$$

where N_μ is the (dead-time-corrected) number of muon stops in the target, $f_{\rm cap}$ is the fraction of muons that undergo nuclear muon capture, $D(E_\gamma, E)$ is the detector response function (i.e., the relative probability of a photon with energy E_γ being reconstructed at an energy E), and $\epsilon\Omega(E_\gamma)$ is the absolute photon detection efficiency for photons of energy E_γ. This absolute photon detection efficiency is the efficiency with a given set of amplitudes on the cathode pads, and so it implicitly accounts for the rate effect. The factors $D(E_\gamma, E)$ and $\epsilon\Omega(E_\gamma)$ and their uncertainties have been discussed earlier. The factor $f_{\rm cap}$, the fraction of muons that undergo OMC in the target, is taken from the literature, and the values used are listed in Table VI. Equation (13) implicitly defines the observable $d\Lambda(E_\gamma)/dE_\gamma$ in terms of known and measured quantities.

N_μ was determined from the number of LT (i.e., the number of dead-time corrected STOP's) after correcting for pileup of the incident muons (a 1.7% effect at the highest rate used), as well as for muons that stopped in the IA counters but were identified as stops in the target due to inefficiency in these counters (a 0.8 to 1.4% effect, depending on the target). The error in N_μ due to these corrections was 0.3 %. The values of N_μ for each target and converter thickness are given in Table VII.

TABLE V. Experimental radiative pion capture branching ratios. For CH_2 the branching ratio listed is $W(CH_2)$, the fraction of π^-'s that capture on hydrogen. The branching ratios are normalized to the branching ratio for ^{12}C.

Target	Branching ratio (%)	Reference
^{16}O	2.24 ± 0.48	45
	2.20 ± 0.33	45
	2.27 ± 0.24	76
	2.17 ± 0.20	present work
^{40}Ca	1.82 ± 0.15	45
	1.94 ± 0.35	77
	1.78 ± 0.15	present work
CH_2	1.26 ± 0.12	50, 51, 52, 53, 45
	1.49 ± 0.14	present work

TABLE VI. The fraction of muons that undergo OMC in the target.[61]

Target	$f_{\rm cap}$ (%)
^{12}C	7.67 ± 0.06
^{16}O	18.38 ± 0.11
^{40}Ca	85.0 ± 0.2

The number of photon events above an observed energy of 57 MeV

$$N^\gamma_{>57} = \int_{57} dE \frac{dN_\gamma(E)}{dE} \tag{14}$$

can be considered as a function of the theoretical partial branching ratio

$$R_\gamma = \int_{57} dE_\gamma \frac{d\Lambda(E_\gamma)}{dE_\gamma} \quad , \tag{15}$$

which is given in units of photons/capture. Alternatively, $N^\gamma_{>57}$ can be considered as a function of g_p. Thus g_p (R_γ) can be determined by comparing the number of photons predicted in the experimental spectrum (above 57 MeV) for a given g_p (R_γ) to $N^\gamma_{>57}$. We refer to this as the "integral method." For a given calculation of the nuclear response, the theoretical photon energy spectrum was convoluted with the detector acceptance and response function and then multiplied by N_μ to give the predicted number of counts above 57 MeV. Simple polynomial fits were made to the predicted $N^\gamma_{>57}$ as a function of R_γ and as a function of g_p/g_a; these were compared to the measured $N^\gamma_{>57}$ to determine g_p/g_a and R_γ.

The second method used to extract R_γ and g_p/g_a from the data was the "spectrum-fitting" method. In this method, a χ^2 fit of the theoretical photon energy spectrum was made to the experimental spectrum, with the normalization of the theoretical spectrum as the free pa-

TABLE VII. The values of N_μ, the dead-time-corrected number of muon stops in the target, and $N^\gamma_{>57}$, the number of photons observed with energies above 57 MeV, after background subtraction.

Target	Converter (mm)	N_μ (10^{10})	$N^\gamma_{>57}$
^{12}C	0.6	12.182 ± 0.038	116 ± 16
	1.0	30.851 ± 0.092	497 ± 43
^{16}O	1.0	20.358 ± 0.061	361 ± 34
^{40}Ca	0.6	7.407 ± 0.022	1299 ± 88
	1.0	9.635 ± 0.029	2159 ± 134

rameter. The theoretical branching ratio for the particular spectrum was then multiplied by this normalization factor to give the experimental branching ratio R_γ. In the cases where the χ^2 per degree of freedom of the fit was significantly larger than 1, the error on the normalization factor from the fit was scaled up by $\sqrt{\chi^2}$. Since the errors on the individual channels in the energy spectrum do not include the systematic errors (due to the normalization of the acceptance, the rate dependence, N_μ, etc.), the error from the χ^2 fit was added in quadrature to these other errors to obtain the total error on R_γ. The value of g_p/g_a was then obtained from R_γ using a polynomial fit of the theoretical branching ratio as a function of g_p/g_a.

The number of photons observed above 57 MeV for each target ($N^\gamma_{>57}$) was corrected for each of the various backgrounds, as discussed earlier. $N^\gamma_{>57}$ was also corrected for the number of otherwise valid photons that were rejected by the trigger electronics. Photons could be rejected due to one of three causes: random vetoing from the IA and IB counters, vetoing from the prompt cut, and finally, the finite length of the LT gate. The first of these effects was calculated from the singles rates in the IA and IB counters. The other two effects were calculated by Monte Carlo. These two corrections were relatively small (7–10 % in total) at the rates used. The uncertainty on these corrections was estimated by varying the parameters used in the Monte Carlo (e.g., the beam rate, muon lifetime, LT gate width, width of the prompt veto) by reasonable amounts, and was found to be $\sim$ 1%. The calculation was checked by examining the energy spectrum of photons rejected by the prompt cut. The fraction of RMC photons rejected by the prompt cut could be estimated by making an approximate subtraction of the radiative pion capture contribution, and was in good agreement with the Monte Carlo calculation.

The values of $N^\gamma_{>57}$ for each target and converter thickness are given in Table VII. The error in $N^\gamma_{>57}$ for each case includes the errors due to the above corrections, as well as errors from three other sources (Table VIII). These are the rate dependence of the acceptance, the energy calibration and the effect of photon absorption in the target. The uncertainty in the energy calibration at 57 MeV (±400 keV) contributes to the error in $N^\gamma_{>57}$. This error was taken as the number of events within 400 keV of the nominal 57 MeV cutoff, and was typically 2–4 %. The error due to photon absorption in the target was determined using GEANT in the same manner as for the pion calibration data, and was typically ~2%, depending on the target. The various contributions to the error in $N^\gamma_{>57}$ are detailed in Table VIII.

V. RESULTS

Figure 15 shows the photon energy spectra, after all cuts, obtained using the 1.0-mm converter. The data obtained with the 0.6-mm converter are similar. As one moves to lower-Z targets fewer muons capture and more decay, hence the RMC signal (in the region from about 53 to 100 MeV) decreases relative to the background due to bremsstrahlung of electrons from muon decay (below 53 MeV), as is obvious from the figure.

A. Calcium

The photon energy spectra from ^{40}Ca obtained with the 0.6 mm and 1.0 mm converters are compared with the theoretical energy spectra from Christillin[22] and Gmitro, Ovchinnikova, and Tetereva[27] in Fig. 16. The theoretical spectra have been convoluted with our detector response function. The errors shown on the data are the statistical errors only. The data taken using the 0.6-mm converter have somewhat poorer statistics but better energy resolution than the 1.0-mm converter data.

Figure 17 shows the predicted value of $N^\gamma_{>57}$ as a function of g_p/g_a and of R_γ. Also shown in these figures is a hatched region which represents the observed $N^\gamma_{>57}$, which corresponds to the area under the experimental spectrum above 57 MeV. The experimental error indicated by the hatched region includes the errors on $N^\gamma_{>57}$, N_μ, and the normalization of the acceptance, added in quadrature and thus includes *all* the contributions to the experimental error.[54] The values of R_γ and g_p/g_a extracted using Fig. 17 (the integral method) are given in Table IX. The fits obtained using the spectrum fitting

TABLE VIII. Contributions to the error in $N^\gamma_{>57}$. All errors are listed in % of $N^\gamma_{>57}$. The total error was obtained by adding the contributing errors in quadrature.

Source of error	^{40}Ca		^{16}O	^{12}C	
	1.0 mm	0.6 mm	1.0 mm	1.0 mm	0.6 mm
Statistics	2.2	2.8	5.5	4.5	9.3
Rate effect	4.7	5.2	5.8	5.5	7.6
Radiative pion capture	~ 0	~ 0	0.01	0.14	0.01
Cosmic rays	0.02	0.03	0.14	0.2	0.2
Bremsstrahlung	0.04	0.07	1.2	3.0	4.9
μ stops outside target	0.2	0.2	0.8	1.8	1.8
Energy calibration	2.6	2.3	3.4	2.7	2.4
Photon absorption in target	2.0	2.0	2.3	2.1	2.1
PROMPT and finite LT	0.9	0.9	1.2	1.1	1.1
total	6.2	6.8	9.4	8.6	13.5

TABLE IX. The partial branching ratio R_γ and g_p/g_a for ^{40}Ca determined using the integral method and the spectrum-fitting method (see text). "Chr" refers to the theory of Christillin[22] and "GOT" refers to the theory of Gmitro, Ovchinnikova, and Tetereva.[27]

Theory	Converter (mm)	Integral R_γ (10^{-5})	Integral g_p/g_a	Spectrum fitting R_γ (10^{-5})	Spectrum fitting g_p/g_a	χ^2_{DOF}
Chr	1.0	2.24 ± 0.17	5.9 ± 0.8	2.19 ± 0.18	5.7 ± 0.8	1.39
	0.6	2.13 ± 0.17	5.4 ± 0.8	2.07 ± 0.18	5.2 ± 0.8	0.80
	average	2.18 ± 0.16	5.7 ± 0.8	2.13 ± 0.16	5.4 ± 0.8	
GOT	1.0	2.08 ± 0.15	$5.1^{+1.8}_{-2.0}$	2.02 ± 0.16	4.4 ± 2.0	1.93
	0.6	2.00 ± 0.14	$4.1^{+1.8}_{-2.0}$	1.90 ± 0.15	2.7 ± 1.9	1.46
	average	2.04 ± 0.14	$4.6^{+1.7}_{-1.8}$	1.96 ± 0.15	3.6 ± 1.9	

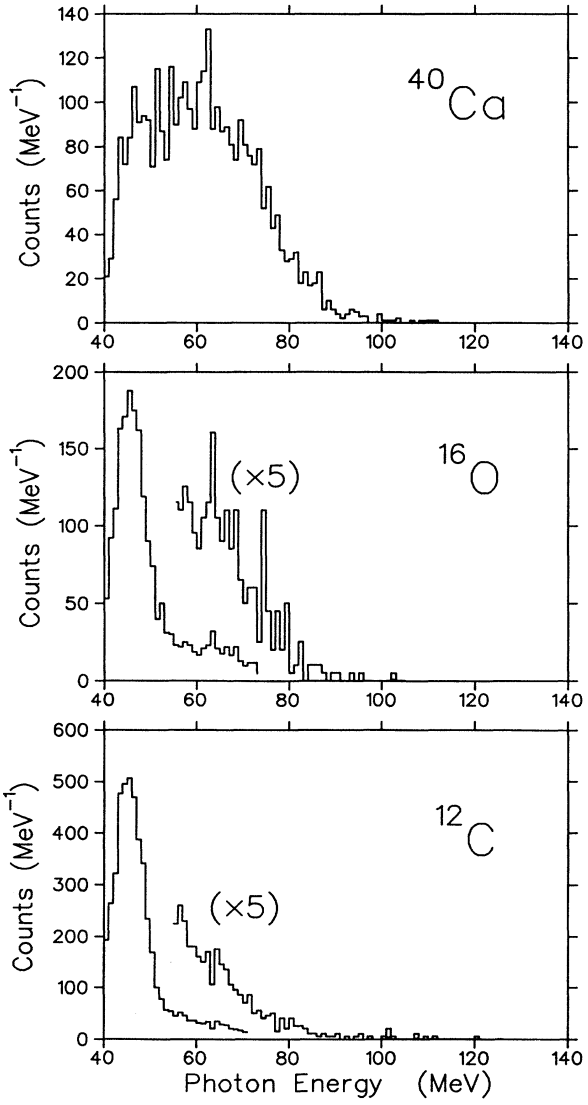

FIG. 15. Photon energy spectra after all cuts, for ^{40}Ca, ^{16}O, and ^{12}C, obtained with the 1.0-mm converter. For the latter two targets, the region below about 53 MeV is dominated by the background due to bremsstrahlung of muon-decay electrons.

method are shown in Fig. 18 for the 1.0-mm converter data (the results obtained with the 0.6-mm converter are similar). The values for R_γ and g_p/g_a obtained using this method are also given in Table IX. The results for both R_γ and g_p/g_a obtained using the two methods are quite consistent (Table IX). The consistency between the two data sets taken using the two different converters is also apparent. These data had different acceptances and resolutions, and were taken during different running periods at different beam rates. The agreement adds confidence in the method of data analysis and the error estimates. A weighted average of the results for the two converters is also given in Table IX. The error on the weighted average has been calculated taking into account the fact that the two measurements are not independent, but have several correlated errors, e.g., the errors on $\epsilon\Omega$, $f_{\rm cap}$, etc.

The results for both the partial branching ratio (R_γ) and for g_p/g_a are in agreement for the two theories, although a slightly smaller branching ratio and g_p/g_a value are obtained using the theory of Gmitro, Ovchinnikova, and Tetereva [27]. It is interesting to note that the reasonable agreement between the values for g_p/g_a for the two theories is somewhat fortuitous, as the two calculations "cross" near the experimental value of $N^\gamma_{>57}$. In fact, for values of g_p/g_a much different than about 7.0, the two theories predict quite different branching ratios. It is also interesting to note that in both cases using the spectrum-fitting method the fit by the theory of Christillin[22] has a somewhat smaller χ^2 than that of Gmitro, Ovchinnikova, and Tetereva.[27] The spectrum-fitting method has the disadvantage that it is more sensitive to inaccuracies in the detector response function or in the input theoretical nuclear response function. Therefore we consider the results obtained from the integral method to be the final results of this experiment. The present results, if compared to closure model calculations (e.g., Refs. 13, 20, and 55) yield very small or even negative values for g_p/g_a.

Table X compares the present results to other recent measurements of RMC on ^{40}Ca. The two earliest experiments are not listed in the table, those of Conversi *et al.*[46] and Rosenstein and Hammerman.[47] Both of these experiments used NaI(Tl) counters without photon converters; consequently, they were troubled by neutron-

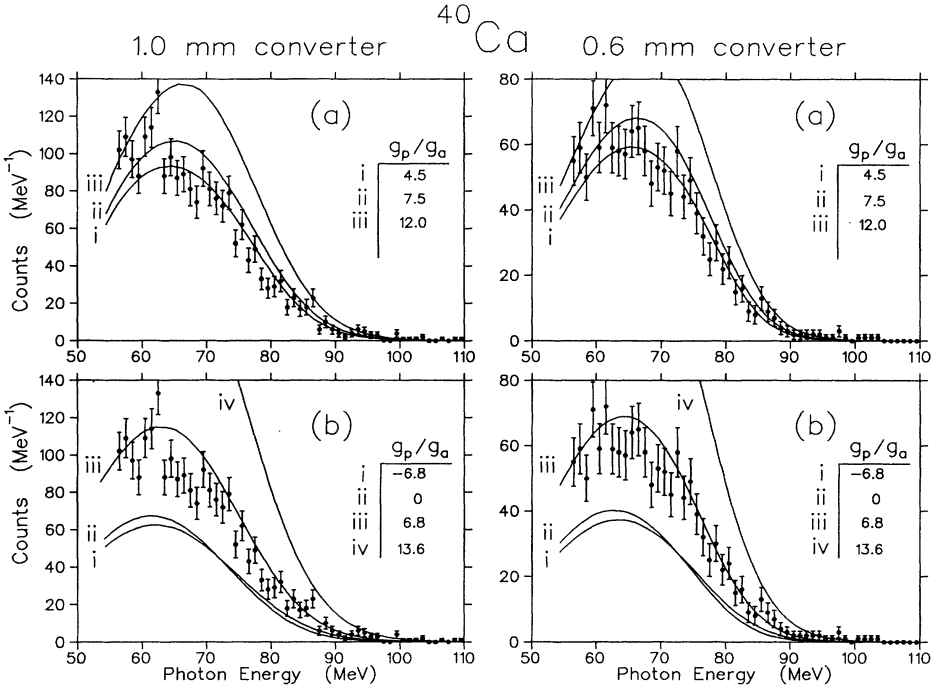

FIG. 16. Photon energy spectrum from ^{40}Ca, compared to the calculations of (a) Gmitro, Ovchinnikova, and Tetereva[27] and (b) Christillin,[22] for different values of g_p. The theoretical spectra have been convoluted with the detector response function. Left: 1.0-mm converter; right: 0.6-mm converter.

induced backgrounds. The present results for R_γ are in good agreement with all the existing data, and are more precise than all except the results of Hart *et al.* However, the error due to the uncertainty in the energy calibration was not included in Hart's error analysis. The present energy resolution is better than all previous experiments except that of Frischknecht *et al.*

Averaging the results of the five experiments listed in Table X gives the value

$$R_\gamma = (2.15 \pm 0.08) \times 10^{-5} \ . \tag{16}$$

Comparing this average result to the phenomenological calculation of Christillin[22] gives the value $g_p/g_a = 5.5 \pm 0.5$ or $(81 \pm 7)\%$ of the PCAC value. Comparing the branching ratio to the MIA calculation of Gmitro, Ovchinnikova, and Tetereva gives $g_p/g_a = 6.0 \pm 1.0$ or $(89 \pm 15)\%$ of the PCAC value. The values for g_p/g_a found using closure model calculations tend to be much

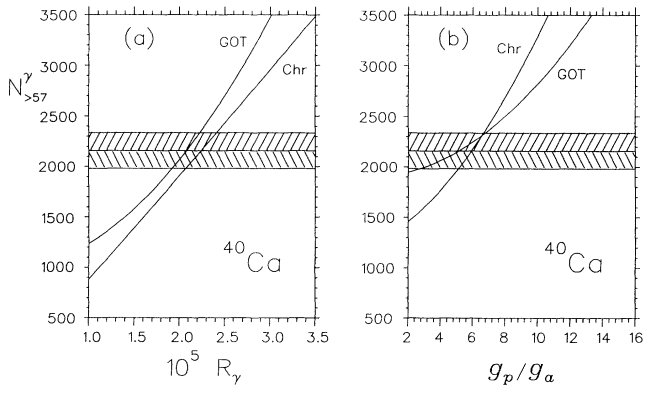

FIG. 17. The number of RMC events from ^{40}Ca ($N^\gamma_{>57}$) as a function of (a) the branching ratio R_γ and (b) g_p/g_a, for the calculations of Christillin[22] ("Chr") and Gmitro, Ovchinnikova, and Tetereva[27] ("GOT"), for the 1.0-mm converter. The hatched area indicates the experimental result.

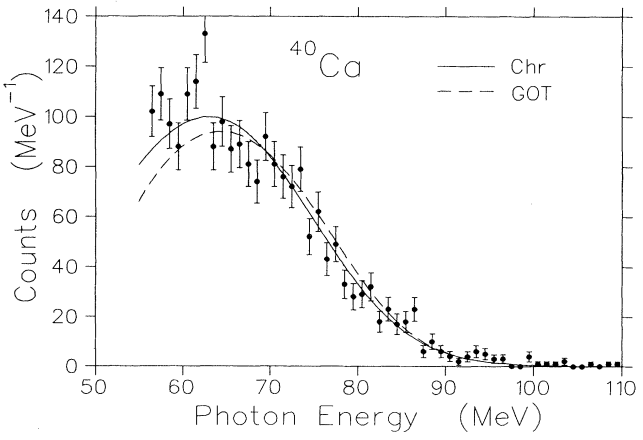

FIG. 18. Photon energy spectrum from ^{40}Ca, compared to the best fits to the theoretical energy spectra from the calculations of Christillin[22] ("Chr") and Gmitro, Ovchinnikova, and Tetereva[27] ("GOT"), for the 1.0-mm converter.

TABLE X. Summary of RMC results for ^{40}Ca from recent measurements. The partial branching ratio R_γ is given in units of 10^{-5}. For theories using the closure approximation, the value of k_{max} found is given. "RYY" refers to the theory of Rood, Yano, and Yano,[78] "Chr" refers to the theory of Christillin[22] and "GOT" refers to the theory of Gmitro, Ovchinnikova, and Tetereva.[27]

R_γ (10^{-5})	Theory	k_{max} (MeV)	No. events	g_p/g_a	Reference
2.11 ± 0.14	RYY	86.5 ± 1.9	1229	6.5 ± 1.6	Hart *et al.*[3]
2.07 ± 0.20			2450		Frischknecht *et al.*[6]
1.92 ± 0.20	RYY	90.8 ± 0.9	2450	3.5 ± 1.3	Frischknecht *et al.*[6]
1.96 ± 0.20	Chr		2450	4.6 ± 0.9	Frischknecht *et al.*[6]
$2.35^{+0.32}_{-0.30}$	Chr		3133	6.5 ± 1.5	Virtue *et al.*[5]
$2.15^{+0.27}_{-0.26}$	GOT		3133	$6.0^{+2.8}_{-2.9}$	Virtue *et al.*[5]
2.30 ± 0.21	Chr		3234	$6.3^{+1.0}_{-1.5}$	Döbeli *et al.*[4,59]
2.18 ± 0.16	Chr		3458	5.7 ± 0.8	present work
2.04 ± 0.14	GOT		3458	$4.6^{+1.7}_{-1.8}$	present work

lower, often leading to (improbable) negative values of g_p/g_a. For both the present results as well as those of Frischknecht *et al.*, the MIA calculation yields a lower value of g_p/g_a if the spectrum-fitting method is used rather than the integral method. If the three values of g_p/g_a extracted in this way from Frischknecht *et al.*, Virtue *et al.*, and the present work are averaged, they give $g_p/g_a = 3.1 \pm 0.6$. However, the χ^2 of the fits tend to be poor. The poorer χ^2 and lower value of g_p/g_a appear to be due to the calculation underestimating the rate at lower photon energies. Frischknecht *et al.* [6] have speculated that this may be due to the fact that quadrupole excitations were omitted in the calculation. Therefore the lower value of g_p/g_a extracted by fitting the theory of Gmitro, Ovchinnikova, and Tetereva to the shape of the spectrum should be viewed with caution.

The recent sum-rule calculations of Roig and Navarro[25] cannot be compared as directly to our data, since predictions of the photon energy spectrum are not yet available. However, the world-average branching ratio given above would imply a value of $g_p/g_a = 8.1 \pm 0.3$, indicating a value larger than the PCAC prediction, in contrast to both the phenomenological and the MIA models.

Measurements of another observable in RMC, the photon muon-spin angular correlation (α_γ) have also been made for ^{40}Ca. Only the results of Hart *et al.*[3] and Virtue *et al.*[56] exist in final form. Unfortunately, these results are not sufficiently accurate to yield meaningful information on g_p.

B. Oxygen

The photon energy spectrum from ^{16}O, along with the fits obtained using the spectrum-fitting method are displayed in Fig. 19. In the same way as for ^{40}Ca, both the integral method and the spectrum-fitting method were used to extract R_γ and g_p/g_a from these data. Figure 20 shows $N^\gamma_{>57}$ as a function of g_p/g_a. Again, the hatched area corresponds to the experimental result with all contributions to the experimental error included. The results for g_p/g_a and R_γ obtained using both the integral method, and the spectrum-fitting method are given in Table XI. The results of the spectrum-fitting method are in excellent agreement with the results of the integral method. As was the case for ^{40}Ca, the integral method results will be considered as the final results.

The extracted branching ratios R_γ using the two theories are in excellent agreement, and yet the values for g_p/g_a are very different. The result of $g_p/g_a = 7.3 \pm 0.9$ using the phenomenological calculation of Christillin and Gmitro[23] is in agreement with the PCAC estimate, but the result $g_p/g_a = 13.6^{+1.6}_{-1.9}$ from the MIA calculation of Gmitro, Ovchinnikova, and Tetereva[27] indicates a large upwards renormalization of g_p in the ^{16}O nucleus. The two calculations are clearly in conflict. The present results for the ^{16}O branching ratio compared to the earlier IA calculation of Gmitro *et al.*[24] (without the continuity equation constraint) would yield $g_p/g_a < 4.0$. The

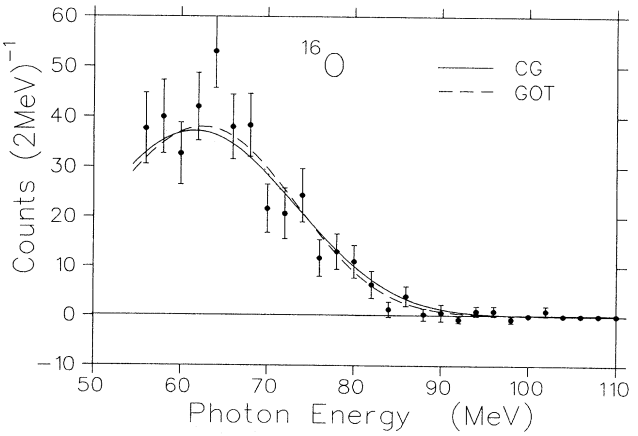

FIG. 19. Photon energy spectrum from ^{16}O, compared to the best fits to the theoretical energy spectra from the calculations of Christillin and Gmitro[23] ("CG") and Gmitro, Ovchinnikova, and Tetereva[27] ("GOT").

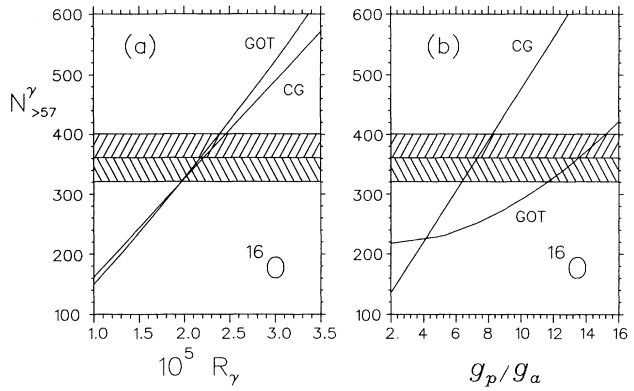

FIG. 20. The number of RMC events from ^{16}O ($N^{\gamma}_{>57}$) as a function of (a) the branching ratio R_γ and (b) g_p/g_a, for the calculations of Christillin and Gmitro[23] ("CG") and Gmitro, Ovchinnikova, and Tetereva[27] ("GOT"). The hatched area indicates the experimental result.

present branching ratio would lead to a negative value for g_p/g_a if compared to the early closure model calculation for ^{16}O of Rood and Tolhoek.[13] When compared to the sum-rule calculation of Roig and Navarro[25] the measured branching ratio indicates the value $g_p/g_a = 9.1 \pm 0.9$.

The present results are compared to the other existing data for RMC on ^{16}O in Table XII. Only two previous measurements exist, both from the Paul Scherrer Institute but using different detectors. Much larger preliminary branching ratios from both of these experiments have been reported [$(6.2\pm0.8)\times10^{-5}$,[57] $(6.5\pm1.3)\times10^{-5}$ (Ref. 58)]. These were discussed in the literature[23,27,16] and the good agreement between them led to the conclusion in a review article by Gmitro and Truöl[16] that there was evidence for a significant upward renormalization of g_p in the ^{16}O nucleus. These results would indicate a value of $g_p/g_a > 16$ when compared to any of the recent calculations of the nuclear response.[23,27,25] However, both of these preliminary results were later found to be in error,[4,7] and they have been superseded by the results given in Table XII.

The present results for R_γ are more precise than either of the previous measurements, both of which were troubled by very large backgrounds from radiative pion capture [in both cases, the background from (π^-,γ), after subtraction of prompt events, was comparable with the RMC signal]. Our results are in good agreement with that of Döbeli *et al.*,[4,59] but disagree by $> 3\sigma$ with the final result of Frischknecht *et al.*[57] It should be noted that Döbeli *et al.*[4,59] used a value for $f_{\rm cap}$ (the fraction of muons stopping in ^{16}O that undergo OMC) of $(17.5 \pm 0.5)\%$, based on results summarized by Eckhause *et al.*[60] More recent data are available[61] which yield $f_{\rm cap} = (18.38 \pm 0.11)\%$. This value has been used by Frischknecht *et al.*[57] and in the present work. Applying this value to the result of Döbeli *et al.*[4,59] would reduce their branching ratio by another 5%, which would improve their agreement with the present results.

A firm statement about any possible renormalization of g_p/g_a in ^{16}O away from the PCAC value awaits a clarification of the theoretical situation. The two most recent calculations[23,27] that provide a photon energy spectrum as well as a branching ratio are in disagreement. Unfortunately, it does not appear possible to select between the two calculations by a measurement of the photon muon-spin angular correlation α_γ in ^{16}O. Not only would this pose formidable experimental challenges, but the ratio R_γ/α_γ is not sufficiently different between the two calculations.[62,16] Part of the difference between the two calculations might be attributable to the neglect of quadrupole excitations in the MIA calculation;[27] such excitations contribute $\sim 6\%$ to the radiative rate in the phenomenological calculation. Also, in the MIA calculation, the photon wave was decomposed to single out the gradient term, to allow the imposition of the electromagnetic continuity equation; the use of a different decomposition would also somewhat increase the predicted RMC branching ratio.[27] However, the combination of both of these effects is still not sufficient to reconcile the two calculations. It should be noted that neither calculation can reproduce the RMC branching ratio and the OMC rate simultaneously. The recent sum-rule calculation of Roig and Navarro[25] yields a value for g_p/g_a intermediate between those extracted from the MIA calculation and the phenomenological model, also indicating an enhancement over the PCAC prediction. It is suggestive, however, that the value of g_p/g_a found using the MIA theory is consistent with the values of g_p/g_a (~ 12) determined from the ratio of exclusive OMC and β-decay rates in ^{16}O.[63–65] Perhaps it is relevant that the explicit effects of meson-exchange corrections have been included (to some degree) in both the MIA calculations and the

TABLE XI. The partial branching ratio R_γ and g_p/g_a for ^{16}O determined using the integral method and the spectrum-fitting method (see text). "GOT" refers to the theory of Gmitro, Ovchinnikova, and Tetereva[27] and "CG" refers to the theory of Christillin and Gmitro.[23]

Theory	Integral		Spectrum fitting		
	R_γ (10^{-5})	g_p/g_a	R_γ (10^{-5})	g_p/g_a	χ^2_{DOF}
GOT	2.18 ± 0.21	$13.6^{+1.6}_{-1.9}$	2.13 ± 0.24	$13.1^{+1.8}_{-2.0}$	1.15
CG	2.22 ± 0.23	7.3 ± 0.9	2.16 ± 0.24	7.1 ± 0.9	1.35

TABLE XII. Summary of the results for the partial branching ratio R_γ and g_p/g_a for ^{16}O from all existing measurements. "GOT" refers to the theory of Gmitro, Ovchinnikova, and Tetereva[27] and "CG" refers to the theory of Christillin and Gmitro.[23]

R_γ (10^{-5})	Theory	No. events	g_p/g_a	Reference
3.8 ± 0.4	CG	1400	13.5 ± 1.5	Frischknecht *et al.*[7]
2.44 ± 0.47	CG	325	8.4 ± 1.9	Döbeli *et al.*[4,59]
2.22 ± 0.23	CG	361	7.3 ± 0.9	present work
2.18 ± 0.21	GOT	361	$13.6^{+1.6}_{-1.9}$	present work

calculations used to extract g_p/g_a from the OMC and β-decay data.

C. Carbon

There is only one calculation of RMC specific to ^{12}C available at present that provides a photon energy spectrum, the MIA approach of Gmitro *et al.*[28]. Figure 21 shows the photon spectra for ^{12}C obtained with the 0.6 mm and 1.0-mm converter, compared to the theoretical spectra. As before, the errors on the data include the effect of the subtraction of high-energy tail events from the bremsstrahlung background. The results for R_γ and g_p/g_a are depicted graphically in Fig. 22. The results are tabulated in Table XIII. There is good agreement between the extracted branching ratios from the two data sets (1.0-mm converter and 0.6-mm converter), for both the integral and spectrum fitting methods. However, the branching ratio and the value for g_p extracted using the spectrum fitting method are somewhat lower than those found in the integral method. As exhibited in Fig. 21, the theoretical spectrum underestimates the photon yield below ~ 60 MeV. Whether this is due to an underestimate of the contribution due to bremsstrahlung in the data or a deficiency with the nuclear model is not clear.

Comparing the branching ratio extracted using the integral method to the sum-rule predictions of Roig and Navarro gives $g_p/g_a = 11.4 \pm 0.9$. While this is somewhat less than the value found using the MIA model, it is still much larger than the PCAC prediction.

The only other measurement of RMC on ^{12}C is that of Döbeli *et al.*[4,59] Just as for their ^{16}O data, preliminary results[58] for the partial branching ratio of $(7.4 \pm 1.8)\times10^{-5}$ and the later value[66] of $(10.6 \pm 3.0)\times10^{-5}$ were found to be in error. Again, these preliminary results were quoted in the review by Gmitro and Truöl[16] and were considered by those authors to be further evidence of a systematic renormalization (upwards) of g_p in light nuclei. The final branching ratio obtained, $(2.7 \pm 1.8) \times 10^{-5}$,[4,59] supersedes the preliminary results given above. Only 75 ± 46 events were observed, and the pion-induced background was again large (46% of the RMC spectrum *after* the prompt cut). Though their value for R_γ agrees with the more precise results of the present work, it provides no significant constraints on g_p/g_a.

It is of interest to compare the present results for g_p/g_a to the results of polarization observables in the ordinary muon capture reaction ^{12}C$(\mu^-,\nu)^{12}$B(g.s.). Two measurements exist of P_{av}, the polarization of the re-

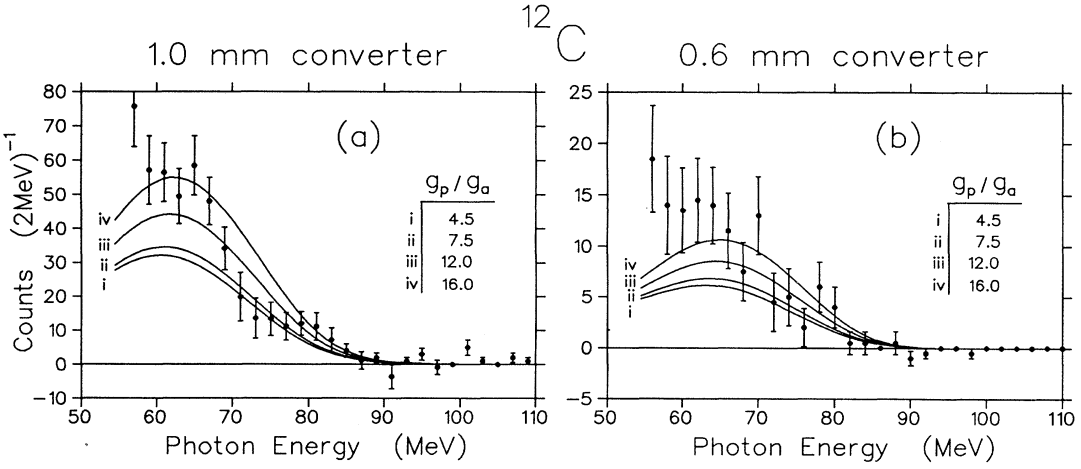

FIG. 21. Photon energy spectrum from ^{12}C, compared to the calculations of Gmitro *et al.*,[28] for different values of g_p. (a) 1.0-mm converter and (b) 0.6-mm converter. The theoretical spectra have been convoluted with the detector response function.

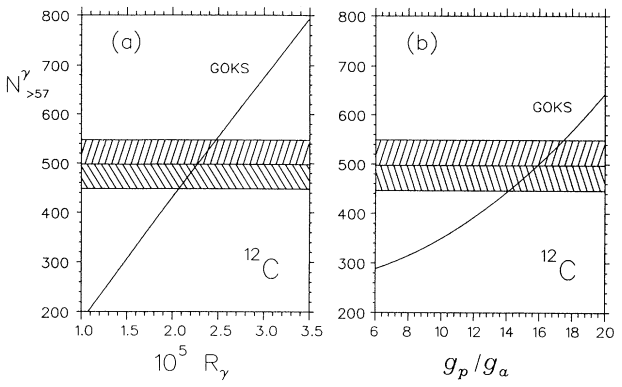

FIG. 22. The number of RMC events from ^{12}C ($N^{\gamma}_{>57}$) as a function of (a) the branching ratio R_γ and (b) g_p/g_a, for the calculation of Gmitro *et al.*,[28] for the 1.0-mm converter. The hatched area indicates the experimental result.

coil nucleus along the muon spin direction, and they are in good agreement.[67,68] When averaged and compared with the calculations of the Osaka group[69,70] they yield $g_p/g_a = 10.2\ ^{+1.6}_{-1.8}$; however, there is an additional uncertainty of about 10% due to the poorly-known capture rates to the various excited states. A somewhat larger value of $g_p/g_a \sim 13.6$ was obtained from the data when compared to the calculation of Parthasarathy and Sridhar.[71] A measurement of $P_{\rm av}/P_L$ also exists, where P_L is the projection of the polarization of the recoiling nucleus along the recoil direction.[72,73] This yields $g_p/g_a = 9.1 \pm 1.8$ when compared to the calculations of the Osaka group,[70] however, the result is still sensitive to corrections due to the excited states. These results tend to indicate an enhancement of g_p over the PCAC value, although not as large as that obtained from the present result. Comparisons of both the MIA prediction of the OMC rate with the measured rate[61] and the RMC branching ratio with the sum-rule calculation[25] indicate a value larger than the PCAC estimate. It is tempting to speculate that the sum-rule calculation, if modified beyond the impulse approximation in a manner similar to that adopted in the MIA approach, might bring the two calculations into better agreement, thereby strengthening the argument for an enhancement of g_p over the PCAC value. However, considering the variance between the two available calculations of RMC in ^{12}C, the possibility cannot be discarded that the enhancement observed is due to deficiencies in the nuclear model.

VI. CONCLUSIONS

The results presented here represent the first measurement of radiative muon capture using a large solid-angle pair spectrometer. The results are largely background free, and the use of two different photon converters for two of the targets provides a valuable check on the systematics.

The branching-ratio results for the ^{40}Ca "test case" are in good agreement with the many previous measurements, and when compared to the two recent calculations indicate a value of g_p/g_a somewhat less than the PCAC value. This could indicate a "quenching" of g_p in the ^{40}Ca nucleus. However, the difference from the PCAC value is of the same order as the difference between the values extracted from the two theories. Also, a comparison of the experimental results to a recent sum-rule calculation indicates that g_p/g_a is somewhat larger than the PCAC value. Thus a definitive statement about any renormalization of g_p in ^{40}Ca awaits more consistency in the theoretical treatment of the nuclear response.

Very different values of g_p are obtained from the present result for ^{16}O when compared to the most recent calculations of the nuclear response. When compared to a phenomenological calculation it yields a value consistent with the PCAC value for g_p; however, when compared to a microscopic calculation it indicates a substantially larger value. An intermediate value is obtained by comparing to a recent sum-rule calculation. Similarly, the data for ^{12}C (which represent the first reliable measurement for RMC on this nucleus) when compared to a similar microscopic calculation yield a value for g_p almost twice the PCAC prediction for the nucleon. The sum-rule calculation also supports a value larger than that given by PCAC. Since the PCAC value is known from ordinary muon capture measurements to be correct at least to within about 25%, the results obtained from the MIA microscopic calculation would seem to require a large enhancement of g_p from its nucleonic value in ^{12}C and ^{16}O. There are indications from some other muon capture experiments that there may indeed be such an enhancement.[65,67,68,74] However, given the difficulties involved with calculating inclusive nuclear RMC, it is by no means obvious that the apparent enhancement is not

TABLE XIII. The partial branching ratio R_γ and g_p/g_a for ^{12}C determined using the integral method and the spectrum fitting method (see text). "GOKS" refers to preliminary results from the calculation of Gmitro *et al.*[28]

Theory	Converter (mm)	Integral R_γ (10^{-5})	Integral g_p/g_a	Spectrum fitting R_γ (10^{-5})	Spectrum fitting g_p/g_a	$\chi^2_{\rm DOF}$
GOKS	1.0	2.27 ± 0.20	$15.9\ ^{+1.5}_{-0.8}$	1.94 ± 0.23	$13.2\ ^{+2.0}_{-2.8}$	1.30
	0.6	2.52 ± 0.34	$17.7\ ^{+2.8}_{-2.4}$	2.08 ± 0.37	$14.5\ ^{+2.2}_{-4.1}$	0.55
	average	2.33 ± 0.17	$16.2\ ^{+1.3}_{-0.7}$	1.98 ± 0.20	$13.7\ ^{+1.7}_{-2.2}$	

an artifact due to problems with handling the nuclear response function. Again, further theoretical work in this area would be welcome.

It is interesting to note, however, that the trend towards a dependence of the radiative muon capture branching ratio R_γ on the atomic number Z, which was suggested by Döbeli *et al.*,[4] is not indicated in the present data. The values determined for R_γ for the three nuclei measured (^{12}C, ^{16}O, ^{40}Ca) are, in fact, nearly identical. Therefore it would be of interest to extend these measurements to nuclei higher in the periodic table.

ACKNOWLEDGMENTS

We thank M. Gmitro for providing us with preliminary results of his group's calculations for ^{12}C, and for useful discussions on the theory of radiative muon capture. We thank H. Fearing and D. Beder for valuable discussions. We are grateful to S. Ball, S. Daviel, and D. Sample for work on software development and A.M. Simard, H. Przysiezniak, and K. Pflug for contributions to aspects of the data analysis. This work was supported by the Natural Sciences and Engineering Research Council of Canada and the U.S. National Science Foundation.

---

[a]Present address: Virginia Polytechnic Institute and State University, Blacksburg, Virginia 24061.
[b]Present address: Rice University, Houston, Texas 77251.
[c]Deceased.
[d]Present address: University of Kentucky, Lexington, Kentucky 40506.
[e]Present address: Buena Vista College, Storm Lake, Iowa 50588.
[f]Present address: Université de Montréal, Montréal, P.Q., Canada H3C 3J7.
[g]Present address: TRIUMF, Vancouver, British Columbia, Canada V6T 2A3.
[h]Present address: Queen's University, Kingston, Ontario, Canada K7L 3N6.
[i]Present address: Atominstitut d. Österr. Universitäten, Vienna, Austria.

[1]G. Bardin, J. Duclos, A. Magnon, J. Martino, A. Richter, E. Zavattini, A. Bertin, M. Piccinini, A. Vitale, and D. Measday, Nucl. Phys. **A352**, 365 (1981).
[2]G. Conforto, M. Conversi, and L. di Lella, Phys. Rev. Lett. **9**, 22 (1962).
[3]R.D. Hart, C.R. Cox, G.W. Dodson, M. Eckhause, J.R. Kane, M.S. Pandey, A.M. Rushton, R.T. Siegel, and R.E. Welsh, Phys. Rev. Lett. **39**, 399 (1977).
[4]M. Döbeli, M. Doser, L. van Elmbt, M.W. Schaad, P. Truöl, A. Bay, J.P. Perroud, J. Imazato, and T. Ishikawa, Phys. Rev. C **37**, 1633 (1988).
[5]C.J. Virtue, Ph.D. thesis, University of British Columbia, 1987.
[6]A. Frischknecht *et al.*, Phys. Rev. C **32**, 1506 (1985).
[7]A. Frischknecht *et al.*, Phys. Rev. C **38**, 1996 (1988).
[8]D.S. Armstrong *et al.*, Phys. Rev. C **40**, R1100 (1989).
[9]D.S. Armstrong *et al.*, in *Weak and Electromagnetic Interactions in Nuclei*, edited by P. Depommier (Editions Frontieres, Gif-sur-Yvette, 1989), p. 637.
[10]M.D. Hasinoff *et al.*, Czech. J. Phys. Proc. Supp. **B39**, 125 (1989).
[11]J. Bernstein, Phys. Rev. **115**, 694 (1959).
[12]G. I. Opat, Phys. Rev. **134**, B428 (1964).
[13]H.P.C. Rood and H.A. Tolhoek, Nucl. Phys. **70**, 658 (1965).
[14]S.L. Adler and Y. Dothan, Phys. Rev. **151**, 1267 (1966).
[15]H.W. Fearing, Phys. Rev. C **21**, 1951 (1980).
[16]M. Gmitro and P. Truöl, Adv. Nucl. Phys. **18**, 241 (1987).
[17]M. Gmitro and A.A. Ovchinnikova, Nucl. Phys. **A356**, 323 (1981).
[18]P. Christillin, M. Rosa-Clot, and S. Servadio, Nucl. Phys. **A345**, 331 (1980).
[19]H.W. Fearing, Phys. Rev. **146**, 723 (1966).
[20]E. Borchi and S. De Gennaro, Phys. Rev. C **2**, 1012 (1970).
[21]P. Christillin, Czech. J. Phys. **B32**, 266 (1982).
[22]P. Christillin, Nucl. Phys. **A362**, 391 (1981).
[23]P. Christillin and M. Gmitro, Phys. Lett. **150B**, 50 (1985).
[24]M. Gmitro, S.S. Kamalov, T.V. Moskalenko, and R.A. Eramzhyan, Czech. J. Phys. **B31**, 499 (1981).
[25]F. Roig and J. Navarro, Phys. Lett. B **236**, 393 (1990).
[26]E.Kh. Akhmedov, T.V. Tetereva, and R.A. Eramzhyan, Yad. Fiz. **42**, 67 (1985) [Sov. J. Nucl. Phys. **42**, 40 (1985)].
[27]M. Gmitro, A.A. Ovchinnikova, and T.V. Tetereva, Nucl. Phys. **A453**, 685 (1986).
[28]M. Gmitro, S.S. Kamalov, F. Šimkovic, and A.A. Ovchinnikova, Nucl. Phys. **A507**, 707 (1990).
[29]N.M.M. Al-Qazzaz *et al.*, Nucl. Instrum. Methods **174**, 35 (1980).
[30]E.W. Blackmore *et al.*, Nucl. Instrum. Methods **A234**, 235 (1985).
[31]The branching ratio for pion charge exchange on the deuteron is more than three orders of magnitude smaller than that on the proton.[75]
[32]C.K. Hargrove *et al.*, Physica Scripta **23**, 668 (1981).
[33]C.K. Hargrove *et al.*, Nucl. Instrum. Methods **219**, 461 (1984).
[34]H. Mes *et al.*, Nucl. Instrum. Methods **225**, 547 (1984).
[35]S. Ahmad *et al.*, Phys. Rev. D **38**, 2102 (1988).
[36]μ^--capture lifetimes are 2.026 μs in ^{12}C, 1.795 μs in ^{16}O, and 333 ns in ^{40}Ca.[61]
[37]D.S. Armstrong, Ph.D. thesis, University of British Columbia, 1988.
[38]R. Poutissou *et al.*, IEEE Trans. Nucl. Sci **30**, 3793 (1983).
[39]R. Brun, F. Bruyant, M. Maire, A.C. McPherson, and P. Zanarini, GEANT3, 1986 (unpublished); CERN Report No. DD/EE/84-1 (unpublished).
[40]J.P. Perroud *et al.*, Nucl. Phys. **A453**, 542 (1986).
[41]J. Spuller, D. Berghofer, M.D. Hasinoff, R. MacDonald, D.F. Measday, M. Salomon, T. Suzuki, J.M. Poutissou, R. Poutissou, and J.K.P. Lee, Phys. Lett. **67B**, 479 (1977).
[42]P. Hanggi, R.D. Viollier, U. Raff, and K. Alder, Phys. Lett. **51B**, 119 (1974).
[43]F. Herzog and K. Alder, Helv. Physica Acta. **53**, 53 (1980).
[44]W. Eichenberger, R. Engfer, and A. van der Schaaf, Nucl. Phys. **A412**, 523 (1984).
[45]J.A. Bistirlich, K.M. Crowe, A.S.L. Parsons, P. Skarek, and P. Truöl, Phys. Rev. C **5**, 1867 (1972).
[46]M. Conversi, R. Diebold, and L. di Lella, Phys. Rev. **136B**, 1077 (1964).

[47]L.M. Rosenstein and I.S. Hammerman, Phys. Rev. C **8**, 603 (1973).
[48]J. van der Pluym, T. Kozlowski, W.H.A. Hesselink, A. van der Schaaf, Ch. Grab, E.A. Hermes, and W. Bertl, Phys. Lett. B **177**, 21 (1986).
[49]F. Sauli, Z. Phys. C **38**, 339 (1988).
[50]M. Chabre, P. Depommier, J. Heintze, and V. Soergel, Phys. Lett. **5**, 67 (1963).
[51]A.F. Dunaitsev, V.I. Petrukhin, and Yu. D. Prokoshkin, Nuov. Cim. **34**, 521 (1964).
[52]D. Bartlett, S. Devons, S.L. Meyer, and J.L. Rosen, Phys. Rev. **B136**, 1452 (1964).
[53]Z.V. Krumstein, V.I. Petrukhin, L.I. Ponomarev, and Yu. D. Prokoshkin, Zh. Eksp. Teor. Fiz. **69**, 1883 (1975) [Sov. Phys. JETP **42**, 955 (1976)].
[54]Due to the energy dependence of the photon acceptance, the same $N^{\gamma}_{>57}$ gives slightly different branching ratios R_{γ} for the two theories. With an energy-dependent acceptance, theoretical energy spectra with different shapes yield different numbers of observed events for the same branching ratio.
[55]R.S. Sloboda and H.W. Fearing, Nucl. Phys. **A340**, 342 (1980).
[56]C.J. Virtue, K.A. Aniol, F.E. Entezami, M.D. Hasinoff, D. Horvath, H.W. Roser, and B.C. Robertson, Nucl. Phys. **A517**, 509 (1990).
[57]A. Frischknecht *et al.*, Czech. J. Phys. **B32**, 270 (1982).
[58]M. Döbeli, M. Doser, L. van Elmbt, M.W. Schaad, P. Truöl, A. Bay, J.P. Perroud, and J. Imazato, Czech. J. Phys. **B36**, 386 (1986).
[59]M. Döbeli, Ph.D. thesis, University of Zurich, 1987.
[60]M. Eckhause, R.T. Siegel, R.E. Welsh, and T.A. Filippas, Nucl. Phys. **81**, 575 (1966).
[61]T. Suzuki, D.F. Measday, and J.P. Roalsvig, Phys. Rev. C **35**, 2212 (1987).
[62]M. Gmitro, S.S. Kamalov, and A.A. Ovchinnikova, Nucl. Phys. **A468**, 404 (1987).
[63]C.A. Gagliardi, G.T. Garvey, J.R. Wrobel, and S.J. Freedman, Phys. Rev. Lett. **48**, 914 (1982).
[64]A.R. Heath and G.T. Garvey, Phys. Rev. C **31**, 2190 (1985).
[65]L.A. Hamel, L. Lessard, H. Jeremie, and J. Chauvin, Z. Phys. A **321**, 439 (1985).
[66]M. Döbeli, M. Doser, L. van Elmbt, M.W. Schaad, P. Truöl, A. Bay, J.P. Perroud, and J. Imazato, in *Weak and Electromagnetic Interactions in Nuclei*, edited by H.V. Klapdor (Springer-Verlag, Berlin, 1986), p. 822.
[67]A. Possoz, Ph. Deschepper, L. Grenacs, P. Lebrun, J. Lehmann, L. Palffy, A. De Moura Gonçalves, C. Samour, and V.L. Telegdi, Phys. Lett. **70B**, 265 (1977).
[68]Y. Kuno, J. Imazato, K. Nishiyama, K. Nagamine, T. Yamazaki, and T. Minamisono, Z. Phys. A **323**, 69 (1986).
[69]M. Kobayashi, N. Ohtsuka, H. Ohtsubo, and M. Morita, Nucl. Phys. **A312**, 377 (1978).
[70]M. Fukui, K. Koshigiri, T. Sato, H. Ohtsubo, and M. Morita, Prog. Theor. Phys. **70**, 827 (1983).
[71]R. Parthasarathy and V.N. Sridhar, Phys. Lett. **106B**, 363 (1981).
[72]L.Ph. Roesch, V.L. Telegdi, P. Truttmann, A. Zehnder, L. Grenacs, and L. Palffy, Phys. Rev. Lett. **46**, 1507 (1981).
[73]L.Ph. Roesch, N. Schlumpf, D. Taqqu, V.L. Telegdi, P. Truttmann, and A. Zehnder, Phys. Lett. **107B**, 31 (1981).
[74]P. Guichon, B. Bihoreau, M. Giffon, A. Gonçalves, J. Julien, L. Roussel, and C. Samour, Phys. Rev. C **19**, 987 (1979).
[75]R. MacDonald *et al.*, Phys. Rev. Lett. **38**, 746 (1977).
[76]G. Strassner *et al.*, Phys. Rev. C **20**, 248 (1979).
[77]H.W. Baer, K.M. Crowe, and P. Truöl, Adv. Nucl. Phys. **9**, 177 (1977).
[78]H.P.C. Rood, A.F. Yano, and F.B. Yano, Nucl. Phys. **A228**, 333 (1974).